Phanerozoic atmospheric CO_2 reconstructed with proxies and models: Current understanding and future directions

Margret Steinthorsdottir[a,b,*], Isabel P Montañez[c,d,*], Dana L Royer[e], Benjamin JW Mills[f], and Bärbel Hönisch[g], [a]Department of Bioinformatics and Genetics, Swedish Museum of Natural History, Stockholm, Sweden; [b]Bolin Centre for Climate Research, Stockholm University, Stockholm, Sweden; [c]Department of Earth and Planetary Sciences, University of California, Davis, CA, United States; [d]UC Davis Institute of the Environment, Davis, CA, United States; [e]Department of Earth and Environmental Sciences, Wesleyan University, Middletown, CT, United States; [f]School of Earth and Environment, University of Leeds, Leeds, United Kingdom; [g]Department of Earth and Environmental Sciences and Lamont-Doherty Earth Observatory of Columbia University, Palisades, NY, United States

Abstract

Knowledge of paleo-atmospheric CO_2 is critical to understanding how Earth System processes respond to a full range of CO_2 concentrations, both past and future. This review addresses the terrestrial and marine proxies used to estimate paleo-CO_2 concentrations and how the biological and/or geochemical properties of each proxy encodes the ambient CO_2 signal, as well as the associated assumptions and uncertainties of the CO_2 estimates. The Phanerozoic history of atmospheric CO_2 is discussed, highlighting a new high-fidelity Cenozoic CO_2 curve and its implications. Subsequently, pre-Cenozoic CO_2 as is currently understood is outlined, in the context of its temporal relationship to climate and evolutionary changes. An overview of carbon cycle modeling for estimating paleo-CO_2 is presented, including the key principles, models, and updates in the field, as well as the key emerging patterns and planned next steps. The review concludes by addressing next steps in advancing the science of CO_2 reconstruction and for improving our understanding of the evolution of atmospheric CO_2 over the past half-billion years.

*Co-lead and co-corresponding authors.

Key points
- Overview the theory of terrestrial and marine paleo-CO$_2$ proxies and the assumptions and uncertainties associated with their CO$_2$ estimates.
- Present the current understanding of Phanerozoic CO$_2$ and highlight the linkages to global surface temperature and major climate and evolutionary changes.
- Discuss the key principles, models and updates in carbon cycle modeling of paleo-CO$_2$ as well as key emerging patterns in modeled CO$_2$ and future directions.
- Address proposed efforts to advance the science of paleo-CO$_2$ reconstruction and for building the next-generation Phanerozoic CO$_2$ record.

Introduction

Atmospheric carbon dioxide concentrations (CO$_2$) have risen >50% above pre-industrial levels, with global annual CO$_2$ concentrations measured at the Mauna Loa Observatories exceeding 420 ppm (422 ppm in July 2023; https://gml.noaa.gov), likely for the first time in over 3 or 4 million years (Tierney et al., 2020; The CenCO$_2$PIP Consortium, 2023). Thus, Earth's climate, forced by increased greenhouse gas concentrations in the atmosphere, is now entering uncharted climatic territory for humankind. This is illustrated by the global temperature anomaly of over 1.2 °C above 1881–1910 baseline values (NASA Giff data) reached in 2016 and again in 2020 (UNFCCC, 2015) and by recent evidence that average temperatures were 1.48 °C above pre-industrial levels in 2023, making it the planet's warmest year on record and perhaps in the last 100,000 years (https://www.copernicus.eu/en). The timing of when the world will achieve net zero carbon emissions and cross the +1.5° to 2 °C climate thresholds set by the 2015 Paris Agreement are topics of much scientific and policy interest and debate (IPCC, 2021, 2022; Palazzo Corner et al., 2023; Tripathy et al., 2023). Some recent studies, including those leveraging artificial intelligence (Diffenbaugh and Barnes, 2023), suggest that Earth will likely cross the 1.5 °C threshold within the next decade and that keeping global warming to below 2 °C is increasingly less likely (Lee et al., 2021; Hansen et al., 2023). Others argue however that maintaining temperatures below 2 °C is still feasible and dependent on when net zero carbon emissions are reached (IPCC, 2021; Palazzo Corner et al., 2023, Michael Mann blog: https://michaelmann.net/content/comments-new-article-james-hansen). This uncertainty in when critical global thresholds will be reached makes constraining how future impacts of global warming will play out a major scientific challenge. Climate proxy records obtained from geological archives provide the opportunity to study Earth System behavior during past CO$_2$-driven climate change and future Earth near-analogues to better understand the aforementioned issues.

Quantitative paleo-CO$_2$ estimates with well-constrained uncertainties are thus fundamentally important to researchers in numerous disciplines because CO$_2$ and planetary function are intrinsically linked. Well-constrained paleo-CO$_2$ records are necessary for validating and parameterizing climate (Caballero and Huber, 2013; Hollis et al., 2019; Anagnostou et al., 2020; Zhu et al., 2020; Tierney et al., 2020), and for ecosystem models utilized to assess ecosystem—CO$_2$ linkages and physiological thresholds for CO$_2$ (e.g., Ibarra et al., 2019; Gurung et al., 2022; Matthaeus et al., 2023). They are crucial in the quest to constrain the magnitude and state-dependency of equilibrium climate sensitivity (ECS), currently broadly constrained at between 2°°C and 4.5 °C (Sherwood et al., 2020; IPCC, 2022), but likely higher in warmer climates (Caballero and Huber, 2013; Friedrich et al., 2016; Zhu et al., 2019). Paleo-CO$_2$ records are further important for advancing our understanding of long-term climate (Earth System) sensitivity (ESS) (Royer et al., 2007; Wong et al., 2021; The CenCO$_2$PIP Consortium, 2023), global biogeochemical cycles, and for exploring interactions within the Earth System, including the biosphere, atmosphere, lithosphere and hydrosphere (Goddéris and Donnadieu, 2019; McKenzie and Jiang, 2019; Tierney et al., 2020; Goddéris et al., 2023). Advancing deeper understanding of CO$_2$-forced changes and consequences is additionally of societal importance, given that the time scales of environmental impacts, socio-economic implications, and mitigation strategies scale to Earth's sensitivity to CO$_2$ concentrations (Hope, 2015).

Multiple reconstructions of the evolution of atmospheric CO$_2$ over the past 400+ Myr have been developed based on compilations of proxy data as well as using geochemical models (e.g., Berner, 1991, 2006a; Berner and Kothavala, 2001; Foster et al., 2017; Lenton et al., 2018; Mills et al., 2019, 2021). Although broad patterns of CO$_2$ have emerged, paleo-CO$_2$ estimates are not always consistent and diverge significantly during some intervals. Possible sources of these inconsistencies are numerous and differ between proxies (see supplemental materials to The CenCO$_2$PIP Consortium, 2023). A major factor, common to many proxies, is uncertainty about how environmental and ecological drivers affect the CO$_2$ proxy signal. Constraining these parameters

typically requires the use of additional proxy records with their own levels of uncertainty. These challenges of proxy-enabled CO_2 reconstructions can lead to a number of assumptions that increase in volume as proxies are applied further back in time. Because these limitations are well recognized by paleoclimatologists, the past decade has nonetheless produced significant advances in deep-time proxy validation and application, including comparison of proxy measurements from co-existing (extinct and/or extant) species, better characterization of environmental background data, such as the elemental and isotopic composition of seawater and atmosphere, and development of proxy system models, as well as efforts to increase the temporal resolution of reconstructions (e.g., The CenCO₂PIP Consortium, 2023).

Here we present a review of the current state-of-the-art, progress made, and challenges remaining in paleo-CO_2 reconstruction using models and proxies. We also present opportunities for further improving the quality and accuracy of paleo-CO_2 estimates. Following the introduction (Section "Introduction"), we outline how past CO_2 can be reconstructed using proxies, explaining the mechanisms and methods involved for each of the most prevalent marine and terrestrial CO_2 proxies (Section "Proxy approach to paleo-CO_2 reconstruction"). Next, Phanerozoic CO_2 history as currently understood is discussed in Section "current status of paleo-co₂ reconstructions", highlighting first a new high-fidelity Cenozoic record based on thorough proxy vetting and modern proxy theory (The CenCO₂PIP Consortium, 2023) and then focusing on the pre-Cenozoic CO_2 and climate evolution. This is followed by an overview of carbon cycle modeling as a means to estimate paleo-CO_2, including the key principles, models and updates in the field, as well as the key emerging patterns and planned next steps (Section "Estimating paleo-CO_2 with long-term carbon cycle models"). Finally, we summarize the state of the art in Phanerozoic CO_2 reconstruction with proxies and models, and list planned future efforts to further improve our understanding of the Phanerozoic CO_2 record and its relationship to paleoclimate (Section "Summary and future directions for paleo-co₂ reconstruction").

Proxy approach to paleo-CO₂ reconstruction

Ice cores provide direct measurements of paleo-CO_2, but this archive is limited to the last 800 ka with isolated intervals of data back to 2 million years, during which time CO_2 consistently remained below 300 ppm (Bereiter et al., 2015; Higgins et al., 2015; Yan et al., 2019). To explore 'future-equivalent' periods in the more distant past, where CO_2 and temperatures were highly elevated, indirect proxies are required to assess paleo-CO_2. Proxies utilize the biological and/or geochemical properties of fossils and minerals that are known to respond to ambient CO_2 when they lived or were formed. Each is associated with different assumptions, degree of understanding, and levels of estimation uncertainty. Paleo-CO_2 proxies have increased in their sophistication over the past several decades and modern approaches involve more highly parameterized inverse models that use proxy data as the input and work backwards to estimate the conditions that produced those observations. Because of these advances in some methods, many published CO_2 records would benefit significantly from being re-evaluated.

Paleo-CO_2 can be inferred from both terrestrial and marine archives (Fig. 1). Marine proxies include the phytoplankton and boron isotope proxies and terrestrial proxies include stomatal frequencies, leaf-gas exchange and leaf-carbon isotopes, as well as the carbon isotopic composition of paleosols (ancient soils) and their occluded organic matter, and the carbon isotopes of liverworts and soil-formed (pedogenic) goethite. Given the relative sparsity of seafloor records older than 200 Ma and significant plankton evolution since this time (Jurassic Period), application of the two marine proxies has largely focused on the Cenozoic. Conversely, terrestrial proxies have been applied through to early Paleozoic (440 Ma) and even Precambrian geologic records (Somelar et al., 2020), including the less extensively used liverwort $\delta^{13}C$ proxy and the $\delta^{13}C$ of pedogenic goethite. Here, we briefly overview the potential and challenges of the commonly used proxies for paleo-CO_2 reconstruction. For a comprehensive review of the marine and terrestrial proxies as well as new advances, and discussion of the sources and scales of uncertainty associated with individual paleo-CO_2 estimates, the reader is referred to the supplemental materials of The CenCO₂PIP Consortium (2023) and www.paleo-co2.org.

Marine paleo-CO₂ proxies

Two types of marine proxies are utilized for reconstructing paleo-CO_2 using geological materials deposited in open ocean regions. The first utilizes the carbon isotopic composition of the organic remains of marine algae (Fig. 1A), whereas the second explores the concentration and isotopic composition of boron incorporated into the fossil shells of calcifying organisms (Fig. 1B). Of the boron proxies, the more commonly used and better understood proxy for reconstructing paleo-CO_2 is the boron isotopic composition.

Phytoplankton proxy

Phytoplankton (marine algae) photosynthesis fractionates carbon isotopes by preferentially assimilating the lighter ^{12}C isotope over ^{13}C in the photosynthate, with the magnitude of fractionation signal (ε_p) increasing with increasing dissolved CO_2 in surface seawater ([CO_2aq]; Fig. 1A). Assuming that CO_2 diffuses passively from seawater into the algal cell, the carbon isotope fractionation associated with the carbon fluxes in and out of the cell thus would be mostly controlled by [CO_2aq] (Freeman and Hayes, 1992; Pagani et al., 2002). The higher the CO_2, the more selective the algae can be and the lower the carbon isotopic composition of algal matter ($\delta^{13}C_{phyto}$) (Rau et al., 1996). This fractionation, ε_p, is stored in organic biomolecules, such as alkenones of coccolithophorid algae, which can be retrieved from ocean sediments. Although alkenones have been used
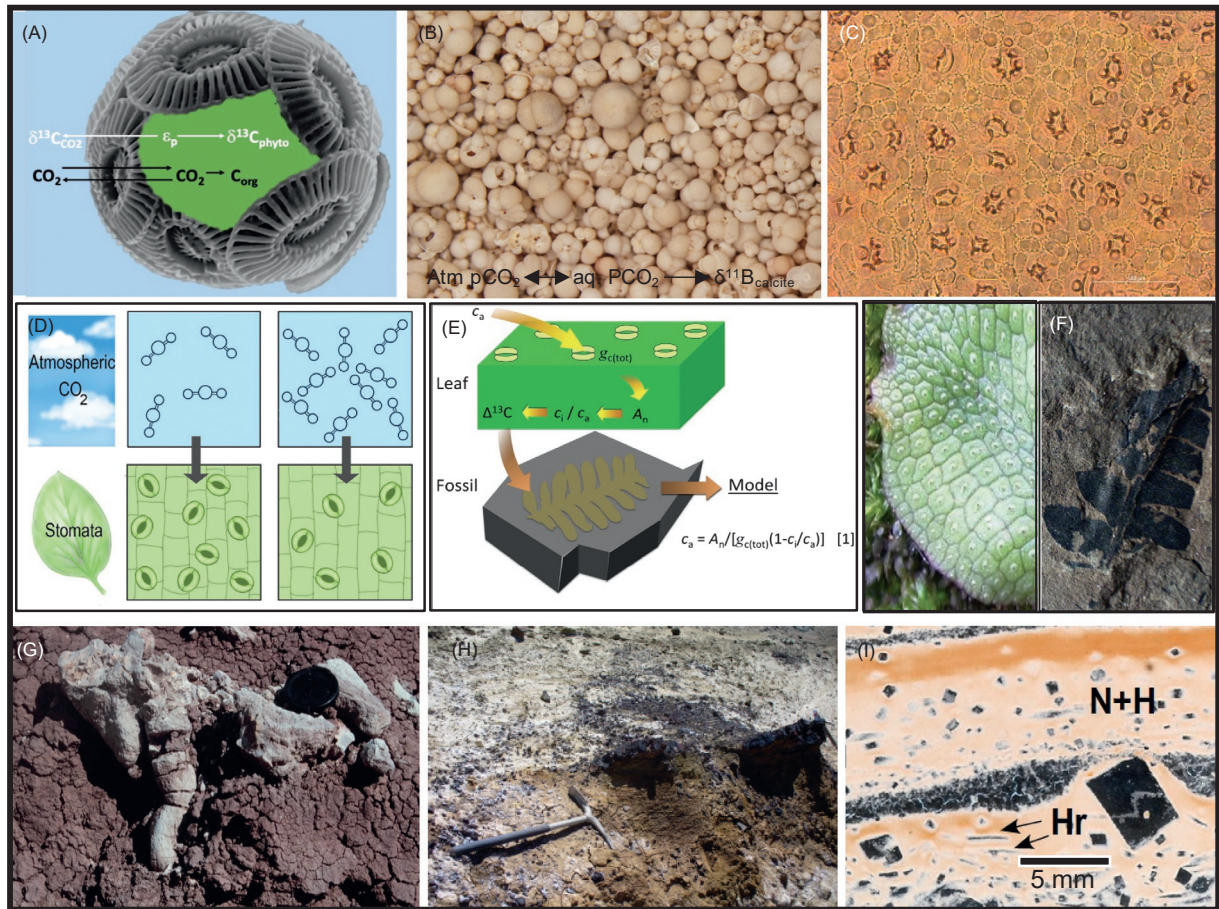
Fig. 1 Compilation of marine and terrestrial CO_2 proxies. (A) Phytoplankton $\delta^{13}C$ proxy relating the $\delta^{13}C$ of algae biomarkers to the $\delta^{13}C$ proxy of the aqueous carbon source for photosynthesis (ε_p). (B) Boron isotope proxy based on the $\delta^{11}B$ of marine carbonates (e.g., foraminifera shells) that incorporate borate ions and whose $\delta^{11}B$ is pH- and atmospheric CO_2-dependent. (C) Cuticle of the 'living fossil' *Ginkgo biloba*, modern relative of the CO_2 proxy fossil plant group Ginkgoales, exhibiting epidermal cells and stomata (darker circular patterns). Scale bar is 100 μm. (D) Inverse relationship between stomatal density (SD) and stomatal index (SI) and atmospheric CO_2. (E) Mechanistic CO_2 model based on a universal leaf gas-exchange equation equating the concentration of atmospheric CO_2 to the rate of CO_2 assimilation during photosynthesis (A_n), total leaf conductance to CO_2 ($g_{c(tot)}$) and the gradient between atmospheric and intercellular CO_2 ($C_a - C_i$); from Franks et al., 2014. (F) Terrestrial plant proxies using the $\delta^{13}C$ of plant fossils or bulk organic matter in sediments. Left: liverwort proxy—nonvascular thalloid liverwort with non-stomatal pores through which CO_2 is uptaken; source: https://mdc.mo.gov/discover-nature/field-guide/liverworts. Right: land plant $\delta^{13}C$ proxy—e.g., Medullosan fossil frond. (G) paleosol carbonate CO_2 proxy. Calcite rhizolith that formed around an early Permian C_3 tap root. (H) Soil-formed goethite CO_2 proxy. Sample of bog iron from a late Paleozoic soil, northwestern Argentina. (I) Nahcolite CO_2 proxy. Thin section photomicrograph of primary nahcolite and halite. Inter-layered nahcolite (N) and halite (H) laminae with halite precipitates (cubes and plates) that precipitated as rafts at the air-water interface. Source: Demicco and Lowenstein, 2010.

widely for this purpose (e.g., Pagani et al., 2005), they only evolved during the Cenozoic and may underestimate aqueous PCO_2 (Bolton and Stoll, 2013). Laboratory and field experiments have shown that photosynthetic carbon isotope fractionation (ε_p) is additionally influenced by nutrient concentration, irradiance, cellular growth, calcification rates, carbon source (i.e., CO_{2aq} and/or), and potentially active carbon-concentrating mechanisms (e.g., Burkhardt et al., 1999; Rost et al., 2002). The degree to which these variables affect $\delta^{13}C_{phyto}$, and the degree to which the estimates of these paleo-environmental and biological variables are constrained, contributes to the uncertainties of paleo-CO_2 estimates made using the phytoplankton proxy and are the subject of ongoing research (e.g., Tanner et al., 2020; Stoll et al., 2019; Wilkes and Pearson, 2019; Zhang et al., 2019b, Zhang et al., 2020; Badger, 2021; Phelps et al., 2021).

A universal molecular fossil is phytane, a diagenetic derivative of chlorophyll found in marine deposits and oils of up to 2 billion years of age. Because phytane averages the carbon isotope fractionation of all photosynthesizing organisms present at the time of synthesis, this proxy has been used to reconstruct paleo-CO_2 throughout the Phanerozoic (Witkowski et al., 2018). The ubiquitous presence of chlorophyll in all algae, however, does not allow for the influence of taxon-specific paleo-environmental and biological factors on the proxy signal.

Boron isotope proxy

A second commonly used marine CO$_2$ proxy is the boron isotope composition of the fossil shells ($\delta^{11}B_{calcite}$) of marine calcifying organisms (Fig. 1B). The $\delta^{11}B_{calcite}$, if reconstructed from sea-surface dwelling planktic foraminifera, can be controlled by atmospheric CO$_2$ (Hönisch and Hemming, 2005; Henehan et al., 2013). This proxy is based on the observation that there are only two dominant dissolved boron species in seawater, boric acid (B(OH)$_3$) and the borate ion (), and their relative concentrations change predictably with seawater pH. Boric acid dissociates to borate and H$^+$ ions at higher pH. There are two stable isotopes of boron, of which ^{10}B preferentially resides in the borate ion, and ^{11}B in boric acid. As seawater pH increases, more and more boric acid dissociates and ^{11}B is progressively present as borate ions. Consequently, the boron isotope ratio (^{11}B/^{10}B) of borate ions increases at higher pH and decreases at lower pH. Marine carbonates preferentially incorporate the charged borate ion into their shells, so their B isotopic composition ($\delta^{11}B_{calcite}$) also follows the abundance and isotopic composition of borate ions in seawater as pH changes. In open-ocean regions, the inferred changes in seawater pH can be translated to atmospheric CO$_2$ if air-sea gas exchange of CO$_2$ is in equilibrium (i.e., [CO2aq] = atmospheric pCO$_2$), temperature, salinity, pressure and a second parameter of the marine carbonate system (e.g., alkalinity, dissolved inorganic carbon, calcite saturation) need to be constrained so that the system of equations can be solved for PCO$_2$.

The precision of boron isotope-based paleo-CO$_2$ estimates, in particular going back in time, is influenced by unknown vital effects in extinct taxa on $\delta^{11}B_{calcite}$ (Anagnostou et al., 2016; Henehan et al., 2016; Hönisch et al., 2021) and by the limited understanding of how the boron isotope composition of seawater ($\delta^{11}B_{sw}$), key to translating measured $\delta^{11}B_{calcite}$ to seawater pH, evolved prior to the Cenozoic (e.g., Raitzsch and Hönisch, 2013; Greenop et al., 2017; Lemarchand et al., 2000). Additionally, the lack of independent proxies for alkalinity or dissolved inorganic carbon (DIC) concentration, which are needed to constrain the second parameter of the marine carbonate system, requires knowledge of paleo-seawater conditions that are only weakly constrained, but are known to have varied over the multi-million year timescale, such as the major ion chemistry of the ocean. These issues are the targets of ongoing research. For recent reviews of this proxy see Rae (2018) and Hönisch et al. (2019).

Terrestrial paleo-CO$_2$ proxies

Terrestrial proxies utilize the fossilized cuticles of vascular plant leaves, with some using their C isotopes, or the chemistry of minerals (carbonate and goethite) and organic matter formed in ancient soils (Fig. 1C–H).

Plant-based terrestrial proxies

For the family of proxies that utilize terrestrial fossil plants, there are several approaches. These include three stomatal proxies and two that utilize the carbon isotope composition of plant-derived organic matter. The cuticles, or waxy outermost layer, of a leaf of vascular plants can be exceptionally preserved in the geologic record and preserve casts of stomata and epidermal cells (Fig. 1C). Stomatal pores are the primary conduit for gas exchange between the leaf and atmosphere, thus vascular plants typically optimize the density and size—including active control of opening/closing—of stomatal pores on their leaf surfaces to ensure sufficient CO$_2$ uptake for assimilation, while minimizing water vapor loss. For most C$_3$ plants (gymnosperms), this leads to an inverse relationship between atmospheric CO$_2$ and the stomatal density (SD = N$_{stomata}$/mm^2) as well as the more commonly used stomatal index (SI (%) = N$_{stomata}$/(N$_{stomata}$ + N$_{epidermal\ cells}$) × 100) with an increasing number of stomata on leaves deriving from periods of low CO$_2$ and vice versa for times of high CO$_2$ (Fig. 1D) (Woodward, 1987; McElwain and Steinthorsdottir, 2017).

This inverse relationship is leveraged by three methods to reconstruct the CO$_2$ concentration experienced by the fossil plant. The first is the empirical stomatal ratio method that uses the ratio between the SD or SI of fossil leaves and their nearest living relative (at ambient CO$_2$) to semi-quantitatively determine paleo-CO$_2$ (McElwain, 1998). A second approach uses an empirical transfer function to infer paleo-CO$_2$ that is defined using herbarium or experimental datasets of responses of nearest-living relatives to a range of CO$_2$, which is then used to calibrate the fossil stomatal frequencies (Kürschner et al., 2008; Barclay and Wing, 2016). For extinct plants lacking a nearest-living relative, a nearest living functional equivalent is used (e.g., Montañez et al., 2016). Environmental parameters other than CO$_2$ (e.g. temperature, nutrient availability, water availability) and differences in physiological traits can influence SD and SI and the CO$_2$-stomata relationship varies among taxa (Haworth et al., 2010; Kürschner et al., 2008; Galvao Duarte, 2019; Yoitis and McElwain, 2019).

The third and most recent approach uses a mechanistic model (Fig. 1E) (Franks et al., 2014; see also Konrad et al., 2008) based on a universal leaf gas-exchange equation equating atmospheric CO$_2$ to the rate of CO$_2$ assimilation during photosynthesis (A$_n$). The model describes the leaf assimilation rate (A$_n$) as the product of two factors: the total leaf conductance to CO$_2$ ($g_{c(tot)}$), which can be inferred by measuring fossil cuticle stomatal traits (density, stomatal pore length and guard cell width) and the gradient between atmospheric and intercellular CO$_2$ ($c_a - c_i$), which is inferred from the C isotopic composition of the fossil cuticle and contemporaneous marine carbonate shell. The cuticle δ^{13}C records the degree to which the lighter C isotope (^{12}C) in CO$_2$ is assimilated over ^{13}C during photosynthesis (i.e., degree of carbon isotopic fractionation (Δ^{13}C = δ^{13}C$_{air}$ – δ^{13}C$_{plant}$)) that is controlled ambient CO$_2$, other environmental factors (e.g., precipitation-to-evaporation ratio, irradiance), and evolutionary differences by plant group (Porter et al., 2017). All three methods rely on comparisons between the fossil plants and their nearest living relative or nearest functional equivalent. Thus, the accuracy and precision of stomatal-based CO$_2$ increases when using multiple species or proxies (Montañez et al., 2016; Kowalczyk et al., 2018; Porter et al., 2019; Steinthorsdottir et al., 2021).

Notably, a global study of the living fossil *Ginkgo biloba*, with long evolutionary lineages, documented a robust relationship between ambient CO$_2$ and stomatal frequency using the three stomatal proxy methods, indicating no influence of climate on the stomatal proxy for this taxon (Steinthorsdottir et al., 2022).

C isotope-based proxies

The C isotopic composition of liverworts, one of the oldest groups of land plants (Fletcher et al., 2006, 2008; Kowalczyk et al., 2018), has potential as a paleo-CO$_2$ proxy (Fig. 1F), but the rarity of liverwort fossils in the geologic record makes this a less commonly used terrestrial plant proxy. This proxy is based on the existence in nonvascular liverworts of static pores through which CO$_2$ uptake cannot be actively controlled as opposed to functional stomata as in vascular plants. This physiological characteristic along with the restriction of liverworts to wet environments (i.e., no imprint of water stress on $\delta^{13}C_{plant}$) means that the degree of C isotopic fractionation during photosynthesis ($\Delta^{13}C$) is largely controlled by the concentration of atmospheric CO$_2$ leading to greater fractionation (and lower $\delta^{13}C_{plant}$) under higher CO$_2$.

The land plant carbon isotope proxy (land plant $\delta^{13}C$ proxy) is based on experimental studies that document a hyperbolic relationship between the magnitude of $\Delta^{13}C$ and atmospheric CO$_2$ (Schubert and Jahren, 2012) (Fig. 1F). This CO$_2$ effect on $\Delta^{13}C$ is attributed to changes in photorespiration, and in turn, carbon isotope fractionation (i.e., photorespiration preferentially oxidizes isotopically light carbon initially fixed by the enzyme Rubisco, increasing the $\delta^{13}C$ of the photosynthate and $\Delta^{13}C$) with increasing CO$_2$ (Schubert and Jahren, 2018). The plant $\delta^{13}C$ proxy has been validated against ice core data of the past 100 ka (Schubert and Jahren, 2015), its precision has been evaluated statistically (Cui and Shubert, 2016), and its accuracy has been tested against other paleo-CO$_2$ proxies (Porter et al., 2019). Given that this proxy approach is based on the magnitude of change in $\Delta^{13}C$, paleo-CO$_2$ concentration is typically calculated based on a change in $\Delta^{13}C$ relative to an independent reference $\Delta^{13}C$ estimated for a time for which the paleo-CO$_2$ value is determined using an independent proxy. Overall, the uncertainty on proxy-based CO$_2$ estimates increases at elevated CO$_2$.

The land plant $\delta^{13}C$ proxy has potential for wide applicability given that fossil organic matter is well preserved in terrestrial sediments deep into the geologic record. But there are multiple challenges to applying this proxy for robust paleo-CO$_2$-reconstruction that await future research (e.g., Zhang et al., 2019a). Applying the $\delta^{13}C$ of bulk organic matter, an approach commonly used, integrates carbon from all organic matter in the sediment. But this approach can be limited by multiple factors that influence the magnitude of carbon isotope fractionation. Sedimentary organic matter can include other sources of C than plant-derived and/or include organic matter from plants that utilized different photosynthetic pathways (C$_3$, C$_4$, CAM). And different plant groups, including within C$_3$ plants, exhibit evolutionary differences in $\Delta^{13}C$ (Porter et al., 2017). These can, in turn, lead to considerable differences in absolute values of $\delta^{13}C$ between sources relative to the ambient CO$_2$ $\delta^{13}C$. Furthermore, environmental conditions, including changes in CO$_2$, can lead to changes in leaf structure, stomatal response and CO$_2$ assimilation rate, as well as post-photosynthetic processes that can all influence the magnitude of carbon isotope fractionation by plants, potentially leading to inverse relationships between $\Delta^{13}C$ and ambient CO$_2$ (Kohn, 2016; Porter et al., 2017; Zhang et al., 2019a; Schlanser et al., 2020; Scher et al., 2022). There remains community debate regarding the accuracy and precision of this proxy approach (Lomax et al., 2019; Schlanser et al., 2020; see discussion in Zhang et al., 2019a). This proxy will benefit from future efforts to constrain the magnitude of the CO$_2$ effect on $\Delta^{13}C$, to better understand the $\delta^{13}C_{plant}$ sensitivity to changing environmental conditions (e.g., water availability on the short-term; O$_2$/CO$_2$ on the long-term), taxonomy, and post-photosynthetic processes, and to improve deep-time reference values (see supplemental materials of The CenCO$_2$PIP Consortium, 2023).

Mineral-based terrestrial proxies

There are three terrestrial mineral-based paleo-CO$_2$ proxies, with the paleosol carbonate CO$_2$ proxy (Fig. 1G) far more commonly used than the goethite or gibbsite proxy (Fig. 1H) or the nahcolite proxy (Fig. 1I). The paleosol carbonate paleo-CO$_2$ proxy is based on a CO$_2$ mixing model with two endmembers: (1) soil-respired CO$_2$ produced by plant roots during respiration and by microbial breakdown of soil organic matter, and (2) atmospheric CO$_2$ (Cerling, 1991, 1992). Paleo-CO$_2$ estimates are determined by specifying four variables in a diffusion-production equation (see Cerling, 1999): (1) the $\delta^{13}C$ value of paleo-soil CO$_2$ (i.e., the CO$_2$ in soil pore space), (2) the $\delta^{13}C$ value of the soil-respired CO$_2$, (3) the $\delta^{13}C$ value of the paleo-atmospheric CO$_2$, and (4) the concentration of the paleo-soil CO$_2$. The $\delta^{13}C$ value of calcium carbonate ($\delta^{13}C_{carb}$) precipitated as nodules or around roots (rhizoliths) in modern and ancient soils (paleosols) is controlled by the $\delta^{13}C$ value of the total soil CO$_2$ when the carbonate is formed, and thus $\delta^{13}C_{carb}$ is the measurable quantity influenced by atmospheric CO$_2$. A temperature-sensitive isotope fractionation factor is applied to relate the $\delta^{13}C$ value of the soil carbonate to the soil CO$_2$. The $\delta^{13}C$ value of the soil-respired CO$_2$ is typically based on $\delta^{13}C$ values of bulk organic matter in the paleosol or occluded within the soil carbonates (Montañez, 2013), with or without a correction for occurrence within the organic-rich A or mineral-rich B horizon of soils (Breecker, 2013). There are complications with using bulk organic matter extracted from paleosols as microbial decomposition of soil organic matter, in particular in the A horizon, which leads to ^{13}C-enrichment of the organic matter (1–2‰) (Breecker, 2013. It is thus recommended that organic matter occluded within soil carbonates be used to determine the $\delta^{13}C$ of paleo-soil-respired CO$_2$. The most physically proximal fossil leaf cuticles or coals have also been used in previous studies which can be problematic given taxonomic variability in and environmental influences on plant $\delta^{13}C$ values, as well as thermal enrichment of coal $\delta^{13}C$ values. For paleo-atmospheric CO$_2$, the $\delta^{13}C$ value is inferred from contemporaneous marine carbonates, e.g., planktic foraminifera for the Cenozoic (Tipple et al., 2010), and brachiopods for the pre-Cenozoic (e.g., Ekart et al., 1999; Montañez et al., 2007, 2016; Nordt et al., 2015).

The largest source of uncertainty in paleo-CO$_2$ estimates made using the paleosol carbonate paleo-CO$_2$ proxy is the fourth parameter, the concentration of the paleo-soil CO$_2$ (Breecker, 2013; Montañez, 2013). This reflects the lack of a proxy in ancient soils for total soil CO$_2$ (denoted as S(z))—to which the model results are quite sensitive (i.e., S(z) is the multiplier in the equation). Many studies assumed values based on the mean concentrations of the growing season CO$_2$ in modern soils (e.g., Ekart et al., 1999; Schaller et al., 2011; Schaller et al., 2015). New approaches for estimating S(z) based on modern and Holocene soil studies are increasingly used in paleo-CO$_2$ reconstructions, including a taxonomic soil order-based S(z) (Montañez, 2013), a mean annual precipitation-based S(z) that uses the chemical index of alteration minus potassium (CIA-K) measured in the paleosol of interest (Cotton and Sheldon, 2013), and a depth-to-carbonate accumulating horizon (updated in Breecker and Retallack, 2014). Efforts to improve the precision of S(z) for application to paleosols is a focus of future research by the paleo-CO$_2$ community. The aforementioned values for a given succession of paleosols are applied to a Monte Carlo based model, PBUQ, which propagates the uncertainty associated with all input parameters (Breecker, 2013), to derive paleo-CO$_2$ estimates. Overall, this proxy works best for past periods of high atmospheric CO$_2$ or where concentrations of both atmospheric and soil-respired CO$_2$ are low—i.e., when the ratio of atmospheric CO$_2$ to soil-respired CO$_2$ (i.e., CO$_2$/S(z)) is no less than 0.3 (Breecker, 2010). This avoids the complication created by an imbalance in the parameters (soil-respired and atmospheric CO$_2$) that govern the δ^{13}C value of total soil CO$_2$, which in turn is archived in the paleosol carbonates.

A second mineral-based proxy of paleo-CO$_2$ is the δ^{13}C of soil-formed goethite (Fig. 1H), an iron oxyhydroxide (Yapp and Poths, 1996; Yapp, 2004), with the potential for use of the aluminum oxide gibbsite (Schroeder and Melear, 1999; Tabor and Yapp, 2005). Similar to the paleosol carbonate proxy, for pedogenic goethite, the δ^{13}C value and mole fraction of Fe(CO$_3$)OH is a function of the concentration and δ^{13}C value of the CO$_2$ proximal to the locus of goethite crystallization. But unlike the carbonate proxy, carbon incorporated into the goethite solid solution can derive from either two-components or three-components soil CO$_2$ components, with the latter including CO$_2$ from dissolved carbonate in the soil (Hsieh and Yapp, 1999; Tabor et al., 2004). In addition to the aforementioned complications created by the influence of different processes on the soil CO$_2$ δ^{13}C value, the conditions that promote crystallization of pedogenic goethite (i.e., cool wet climates with fluctuating moisture availability) can induce alternating oxidation and reduction reactions in the soil that lead to changes in the δ^{13}C values of the goethite that are not predicted by the mass balance relationships applied to goethite-based paleo-CO$_2$ reconstructions (Gulbranson et al., 2011). Despite its potential, the goethite paleo-CO$_2$ proxy is a more complicated system for paleo-CO$_2$ reconstruction and has not been widely used.

The third proxy is the occurrence of sodium carbonate mineral nahcolite in ancient alkaline lacustrine deposits (Fig. 1I), which has been proposed as a paleo-CO$_2$ proxy, given that it precipitates from continental saline alkaline water when a threshold concentration of paleo-atmospheric CO$_2$ is reached (Eugster, 1966; Lowenstein and Demicco, 2006; Jagniecki et al., 2015). The nahcolite proxy has only been applied to the Eocene and unlike all other paleo-CO$_2$ proxies, can only constrain minimal CO$_2$ concentrations, not absolute values (Lowenstein and Demicco, 2006; Jagniecki et al., 2015; Demicco and Lowenstein, 2019).

Current status of paleo-CO$_2$ reconstructions

In this section we present recent advances made in the reconstruction of Cenozoic CO$_2$ by an international consortium of researchers, who recently published a data-model integrated record (Section "Current status of Cenozoic CO$_2$"). We then present an overview of our current understanding of pre-Cenozoic CO$_2$ (66–400+ Ma) in the context of linkages to other Earth surface processes and their interactions (Section "Current understanding of pre-Cenozoic CO$_2$"). Subsections of Section "Current understanding of pre-Cenozoic CO$_2$" focus on major intervals and events in Earth history. Section "Estimating paleo-CO$_2$ with long-term carbon cycle models" then compares the proxy record to different model-derived paleo-CO$_2$ trends over the Phanerozoic, including discussion of recent advances and future directions for modeling CO$_2$. Section "Summary and future directions for paleo-Co$_2$ reconstruction" addresses the next steps needed to extend and expand recent advances in paleo-CO$_2$ reconstruction and ultimately build a next-generation Phanerozoic CO$_2$ record.

Current status of Cenozoic CO$_2$

For decades, compiling Phanerozoic paleo-CO$_2$ estimates and curating the data based on published CO$_2$ records was not a communal effort, but individual researchers, foremost Dana Royer, curated a database collecting all published data in one database (Royer et al., 2001, 2004, 2007; Beerling and Royer, 2011; Foster et al., 2017). This allowed the community to analyze their data in context and encouraged a wide-reaching collaborative effort. In 2016, an international consortium of researchers (CenCO$_2$PIP–The Cenozoic CO$_2$ Proxy Integration Project) formed, with expertise in all established terrestrial and marine paleo-CO$_2$ proxies, and jointly started an effort to rigorously document, vet, and, where possible and necessary, recalculate estimates of paleo-CO$_2$ from raw proxy data in order to conform with the latest proxy understanding. The first phase of this effort focused on the Cenozoic Era, i.e., the past 66 million years, and designed detailed templates for documenting paleo-CO$_2$ estimates, including sampling details, raw and auxiliary proxy data, constants, equations and methods used to collect proxy data and compute paleo-CO$_2$. Data sheets of the originally published estimates have been archived in the paleo-CO$_2$ directory of NOAA's National Climatic Data Center (NCDC) and in Zenodo. Following the creation of the data 'archive,' the consortium vetted all published records based on their analytical quality and whether uncertainty estimation was fully developed and comprehensive 95% confidence intervals were quantified.

To address uncertainties, the Cenozoic CO_2 Proxy Integration Project collaboratively assessed and synthesized existing paleo-CO_2 records spanning the Cenozoic. CO_2 and age uncertainties were updated as necessary, to consistently reflect propagated 95% confidence intervals (CIs). CO_2 records were categorized according to the community's level of confidence in each estimate.

The research effort refining estimates of Cenozoic (66–0 Ma) fluctuations of CO_2 concentrations was recently published (The CenCO$_2$PIP Consortium, 2023). Updated graphs and links to view and download the vetted data are available on the CO$_2$PIP project website (paleo-co2.org). The CenCO$_2$PIP Consortium publication (2023) discusses challenges in reconstructing past CO_2 levels using proxies, describes eight different proxies (phytoplankton, boron proxies, liverworts, leaf gas exchange, leaf carbon isotopes, stomatal frequencies, paleosols and nahcolite/trona) as well as the associated methods, all with evolving assumptions. The resulting statistically modeled Cenozoic CO_2 curve (Fig. 2), produced using a Bayesian inversion model, reveals a robust relationship between CO_2 and global temperatures during the Cenozoic Era (The CenCO$_2$PIP Consortium, 2023) and underscores the relevance of investigating paleo-CO_2 and climate to the escalation of present atmospheric CO_2 levels due to human activities, in projecting potential future outcomes. This synthesis of Cenozoic CO_2 facilitates comparison with observations of past climate and ecosystem changes, allowing us to better identify CO_2 thresholds and assess the sensitivity of Earth's climate and biosphere in response to anthropogenic perturbation. However, despite greatly enhancing our knowledge of Cenozoic CO_2 and its relationship with global temperature change and climate sensitivity, data gaps and inconsistencies persist, emphasizing the need for further data collection to create additional comprehensive and community-vetted paleo-CO_2 records. An overview of Cenozoic CO_2 evolution is provided below; for a comprehensive in-depth review see The CenCO$_2$PIP Consortium (2023) and visit the CO$_2$PIP website (paleo-co2.org).

Cenozoic CO_2 evolution is of particular interest to the paleoclimate research community, since during this period (66–0 Ma) Earth's geographical configuration and ecosystem composition approached that of the modern, with several intervals and transitions that may be considered near future-climate analogues. Overall, comparison of the Cenozoic paleo-CO_2 and climate records exhibits strong correlation between them across timescales of 500-kyr to millions of years with an overall cooling trend interrupted by transient climate change episodes (Fig. 2; The CenCO$_2$PIP Consortium, 2023). The early Cenozoic hothouse was characterized by overall high CO_2 concentrations ($\geq$650 ppm), with peak values more than double that of present-day ($>$1000 ppm) during a transient episode of highly elevated temperatures and CO_2, the Paleocene–Eocene Thermal Maximum (PETM) (Zachos et al., 2001; Huber and Caballero, 2011; Cramwinckel et al., 2018; Anagnostou et al., 2020). CO_2 was up to 1600 ppm and global surface temperatures $\sim$12 °C higher than present-day during the Early Eocene Climatic Optimum (EECO, $\sim$53–51 Ma) and then declined to between 800 and 1100 ppm through the remaining Eocene, in tandem with global cooling. This trend was briefly interrupted by another transient rise in pCO$_2$ and warming at $\sim$40 Ma, the Mid Eocene Climatic Optimum (MECO) (Zachos et al., 2001; Cramwinckel et al., 2018).

A decline in atmospheric CO_2 to $<$600 ppm across the Eocene–Oligocene boundary (33.9 Ma) was associated with a climate transition from the mostly ice-free greenhouse world of the earlier Cenozoic to an icehouse world with extensive Antarctic glaciation in the Oligocene (Hutchinson et al., 2021). Specifically, the new Cenozoic CO_2 record suggests a glaciation threshold of $719\ ^{+180}/_{-152}$ ppm (The CenCO$_2$PIP Consortium, 2023). By $\sim$32 Ma (early Oligocene), CO_2 had dropped to $\sim$550 ppm coinciding with the onset of the evolution of the C_4 carbon-concentrating mechanism in terrestrial vascular plants and their subsequent diversification. With the exception of a brief rise in CO_2 to a mean of 500 ppm during the middle Miocene Climatic Optimum (MCO, $\sim$17–14 Ma), marking the last time (14.5–14 Ma) that CO_2 concentrations were consistently higher than present-day,
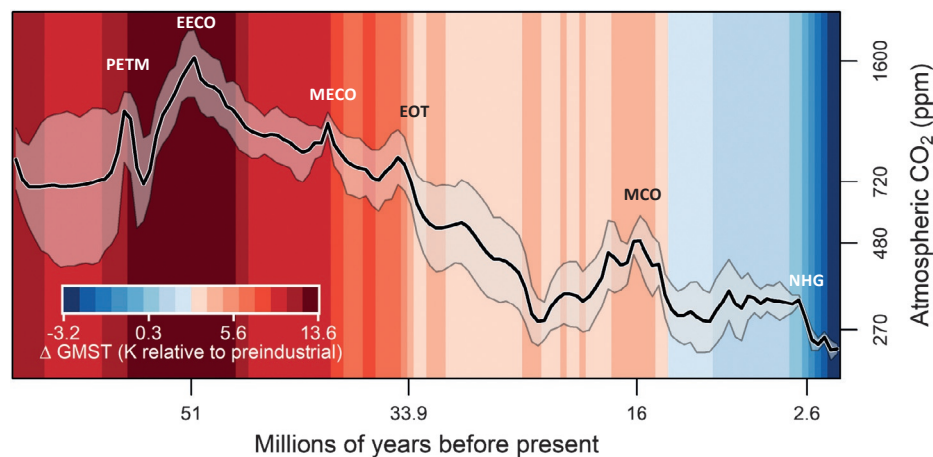
Fig. 2 Statistical reconstruction of the community-vetted CO_2 records ($n = 1673$) over the Cenozoic Era. The paleo-CO_2 curve includes 95% credible intervals and is superimposed on the global mean surface temperature trend (blue and red vertical shading) over the past 66 million years, modeled using the data of Westerhold et al., 2020. Major climate events are highlighted by abbreviations: PETM = Paleocene Eocene Thermal Maximum; EECO = Early Eocene Climatic Optimum; MECO = Middle Eocene Climatic Optimum; EOT = Eocene/Oligocene Transition; MCO = Miocene Climatic Optimum; NHG = onset of Northern Hemisphere Glaciation. Figure modified from The CenCO$_2$PIP Consortium, Science 382: 6675 (2023).

atmospheric CO_2 declined throughout the Neogene (23–2.6 Ma). This CO_2 decline is associated with global cooling. CO_2 and global surface temperature continued to decline into the full-blown ice age world of the Pleistocene (beginning at ~2.65 Ma), when CO_2 dropped below 270 ppm and fluctuated between ~200–280 ppm through the glacial-interglacial cycles (Bereiter et al., 2015).

Current Understanding of pre-Cenozoic CO₂

As we outline throughout this review, the paleo-CO_2 data and model community is presently working on improving the quality and accuracy of CO_2 reconstructions and solving the data-model discrepancies that still exist (see Sections "Key principles" and "Summary and future directions for paleo-co₂ reconstruction"). To date, only Cenozoic CO_2 records have undergone the necessary quality vetting and selection process, whereas updating the pre-Cenozoic CO_2 record is an ongoing effort by the CO_2PIP community (https://paleo-co2.org/co2pip). At this time, the cumulative proxy archive for the Phanerozoic, composed of over 6000 published paleo-CO_2 estimates (Fig. 3), provides a broad-scale perspective of how CO_2 concentrations varied over the past half billion years. To date, this archive has been initially curated using criteria defined by the Cenozoic CO_2PIP Consortium (color symbols on Fig. 3) and used to derive the currently available best-estimate of Phanerozoic CO_2 (Foster et al., 2017). Individual CO_2 records or collections of contemporaneous records provide insight into relative changes in CO_2 during past abrupt and/or major environmental and ecosystem perturbations. Section "Summary and future directions for paleo-CO_2 reconstruction" discusses ongoing efforts to further vet and modernize the pre-Cenozoic portion of this archive.

Below we give an overview of pre-Cenozoic Phanerozoic CO_2 *as currently understood*, placing CO_2 evolution in an Earth System/Carbon cycle context—i.e. the interaction of processes that link the atmosphere, biosphere, hydrosphere and lithosphere and govern CO_2. We focus mostly on terrestrial proxies, which are more numerous in the pre-Cenozoic and note that marine (phytane) and terrestrial proxies largely agree when coeval.

Paleozoic CO₂ (~541–252 Ma)

Proxy-based CO_2 estimates prior to 450 Ma (Cambrian to mid-Ordovician) are lacking but geochemical models consistently predict CO_2 of several 1000s of ppm. Phytane-based estimates indicate Ordovician CO_2 of 300—700 ppm (Fig. 3; Witkowski et al., 2018). The precipitous decrease in CO_2 through the first ~100 Myr of the Paleozoic has been attributed to the evolution and expansion of the earliest land plants, through enhanced oxidative silicate weathering and global increase in organic carbon burial (Lenton et al., 2016; Dahl and Arens, 2020).
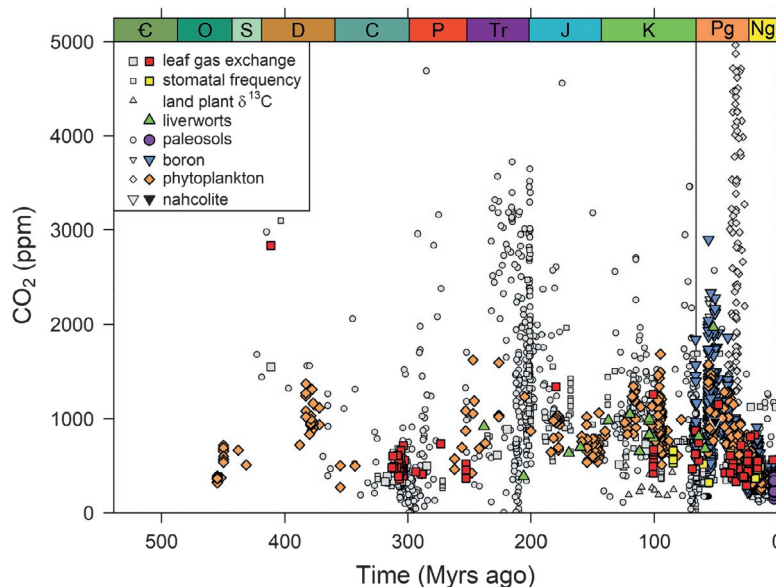
Fig. 3 Phanerozoic compilation of paleo-atmospheric CO_2 estimates with initial vetting of data. All proxy-based CO_2 estimates for the Phanerozoic (4077 data points) are identified by proxy type on the plot by symbol shapes and colors (see legend for details). For the Cenozoic, the colored symbols indicate the highest quality Cenozoic estimates vetted and updated by the CenCO₂PIP Consortium. Colored symbols for the pre-Cenozoic estimates conform to modern proxy understanding, whereas estimates shown in gray are considered unreliable in their current form, either because of analytical concerns, because they are under-constrained with regard to modern proxy understanding, or because their uncertainties are not fully quantifiable. The Phanerozoic system periods are indicated in the colored bar at the top of the graph: C = Cambrian, O = Ordovician, S = Silurian, D = Devonian, C = Carboniferous, P = Permian, Tr = Triassic, J = Jurassic, K = Cretaceous, Pg = Paleogene, Ng = Neogene. Note that the figure is cropped at 5000 ppm CO_2 and does not display 25 (0.6%) of the unreliable CO_2 estimates that exceed this limit.

The geochronologically oldest stomatal proxy-based CO_2 estimates are early Devonian (~419.2–393.3 Ma) and based on the stomatal densities of pre-vascular 'rhynophytic' sporophytes: early free-sporing land plants with anatomical features intermediate between those of bryophytes and tracheophytes. Concentrations of ~2000 to ~3000 ppm are estimated (Fig. 3) using the stomatal ratio method (McElwain, 1998), as well as an early (Roth-Nebelsick and Konrad, 2003) and more recent (Franks et al., 2014) version of a leaf gas-exchange model. Phytane-based CO_2 estimates for the Devonian record a continued drop in CO_2 to values of 300–500 ppm by the close of the Devonian and earliest Carboniferous (~350 Ma; Fig. 4). Paleosol-carbonate proxy estimates of CO_2 for this interval (Mora et al., 1996; Driese et al., 2000; Cox et al., 2001) also record the long-term CO_2 decline with values within the range defined by the phytane proxy estimates.

By the middle Carboniferous (~330 Ma), CO_2 had decreased to overall low concentrations (Fig. 3) coincident with the onset of the late Paleozoic ice age (LPIA, ~340–260 Ma; Montañez et al., 2007; Fielding et al., 2008). Relatively few paleo-CO_2 estimates exist for the early Carboniferous (359–323 Ma) but leaf-fossil proxy-based reconstructions using the stomatal ratio of early conifers (McElwain, 1998), a transfer function applied to arborescent lycopsids (Beerling, 2002), and leaf gas-exchange modeling (Franks et al., 2014) indicate CO_2 of ~300–400 ppm during this time. More recent phytane-based CO_2 estimates (250–400 ppm) further support low concentrations for the early Carboniferous (Witkowski et al., 2018). Less robust paleosol carbonate proxy estimates (category 2 based on the criteria of The CenCO$_2$PIP Consortium, 2023), however, exhibit a much larger range for this interval (negative to ~2000 ppm; Mora et al., 1996; Ekart et al., 1999).

A much higher density of paleo-CO_2 estimates exist for the latter half of the Carboniferous (323–298.9 Ma) and Permian (298.9–251.9 Ma) primarily based on leaf fossil and paleosol carbonate proxies (Fig. 3). Overall proxy estimates define a large range for CO_2 (<100 to ~1000 ppm) throughout this interval (Mora et al., 1996; Ekart et al., 1999; Ghosh et al., 2005; Lucas and Tanner, 2021). Two multi-proxy CO_2 reconstructions (Montañez et al., 2016; Richey et al., 2020) based on stomatal densities and leaf-gas exchange modeling of seed ferns and contemporaneous paleosol carbonates, however, better constrain the evolution of CO_2 over a 40 Myr interval of the late Carboniferous through early Permian (312–275 Ma). These records reveal eccentricity-scale (10^5-year) rhythms of CO_2 fluctuations (Montañez et al., 2016) characterized by ~500–700 ppm during interglacials and ~ 160–300 ppm during glacials with an interval mean of 390 ppm ±130 ppm, mirroring the glacial-interglacial shifts of the Pleistocene ice ages (Montañez et al., 2016; Richey et al., 2020). On the million-year scale, CO_2 decreases through the latest Carboniferous into the earliest Permian reaching a 10-Myr CO_2 nadir (~175–360 ppm) in the earliest Permian (298.9–290.1 Ma); following the nadir, CO_2 increases through to the close of early Permian. A short term (<300 ka in duration) doubling of CO_2 at 304 Ma coincides with an independently identified global warming event, biodiversity nadir, and ~20% of areal extent of seafloor anoxia (Chen et al., 2022). Nadirs of CO_2 in the late Carboniferous coincide with geological evidence of maximum glaciation extent (Montañez, 2022) and the radiation of glossopterids and gigantopterids (McLoughlin, 2012; Zhou et al., 2017). The early Permian CO_2 increase coincides with the onset of widespread volcanism and evidence for increased ice sheet instability (Richey et al., 2020; Montañez, 2022).

Proxy-based records suggest the rise in CO_2 may have continued through the Permian, likely reaching peak values across the Permian-Triassic boundary and into the early Triassic (Fig. 3). All CO_2 estimates for this interval (<400 to ~1800 ppm), and based on the phytane, vetted leaf-gas exchange, liverwort and paleosol carbonate proxies, overlap (Fig. 3). Furthermore, a high-resolution plant $\delta^{13}C$ proxy record across the Permian-Triassic boundary (P–Tr, 251.9 Ma) defines a rapid rise in CO_2 (within 75 kyr) from latest Permian background concentrations of 400–2500 ppm (Wu et al., 2021). Notably, CO_2 estimates based on stomatal frequency and leaf-gas exchange proxies indicate much lower pre-P–Tr boundary CO_2 concentrations (300–500 ppm) (Li et al., 2019). The P–Tr boundary archives the largest mass extinction event in Earth's history leading to extinction of at least 80% and perhaps as much as 96% of all marine species, as well as devastating loss of biodiversity and ecosystem collapse on land (Benton and Twitchett, 2003; Looy et al., 2001; McElwain and Punyasena, 2007; Vajda and McLoughlin, 2007; Stanley, 2016; Vajda et al., 2020). The proposed rapid CO_2 rise across the P–Tr boundary is coincident with a 4–6‰ negative carbon isotope excursion ($\delta^{13}C$) detected in marine and terrestrial deposits globally, hypothesized to record amplification of the transient increase in CO_2 by a catastrophic release of methane from gas hydrate deposits caused by initial climate warming, ultimately leading to a 6–8 °C rise in global temperatures.

Mesozoic CO_2 (252–66 Ma)

The Triassic period

Recovery from the environmental impact of the P–Tr was slow—at the million year-scale—through the Early and Middle Triassic (251.9–237 Ma). Estimates of atmospheric CO_2 through this period range from <100 to 1800 ppm, primarily based on paleosol carbonate and phytane proxy data (Fig. 4; Ekart et al., 1999; Ghosh and Bhattacharya, 2001; Ghosh et al., 2005; Prochnow et al., 2006; Witkowski et al., 2018). Abundant proxy CO_2 data exists for the Late Triassic (237–201.3 Ma) but are poorly constrained to a range of <100 to ~4000 ppm (Fig. 3). Distinct temporal trends in CO_2 exist, however, documenting rapid rises in paleo-CO_2 associated with the emplacement of large igneous province or magmatic arc volcanic activity during the break-up of supercontinent Pangaea (e.g., McElwain et al., 1999; Cleveland et al., 2008; Schaller et al., 2011; Schaller et al., 2015; Steinthorsdottir et al., 2011; Nordt et al., 2015). CO_2 estimates based on the paleosol carbonate, phytane, and stomatal frequency proxies all indicate elevated concentrations during the Late Triassic and a transient doubling across the Triassic-Jurassic (Tr–J) boundary (201.2 Ma). Stomatal frequency (Beerling et al., 1998; McElwain et al., 1999; Steinthorsdottir et al., 2011; Slodownik et al., 2021) and phytane-based (Witkowski et al., 2018) estimates for this interval, however, define a narrower range of CO_2 (~800–1000 ppm and 900–1200 ppm, respectively) than indicated by paleosol carbonate proxy estimates (negative to ~3500 ppm).

The Triassic-Jurassic boundary

The rapid CO_2 rise across the Tr–J boundary was potentially the most significant of the Mesozoic and is attributed to the emplacement of the most extensive continental large igneous province (LIP), the Central Atlantic magmatic province (CAMP; Marzoli et al., 2018), leading to global warming, environmental degradation and culminating in the Triassic–Jurassic mass extinction. Pre-Tr-J event estimates of CO_2 vary from 500 ppm to ~2000 ppm, with higher estimates based on the paleosol carbonate proxy (Ghosh and Bhattacharya, 2001; Tanner et al., 2001; Driese and Mora, 2002; Cleveland et al., 2008; Schaller et al., 2011; Schaller et al., 2015; Whiteside et al., 2015), and lower estimates based on the stomatal frequency (McElwain et al., 1999; Steinthorsdottir et al., 2011) and the liverwort (Fletcher et al., 2008) proxies, albeit with two stomatal frequency-based records (Bonis et al., 2010; Wu et al., 2016) suggesting possible maximum pre-event CO_2 values of up to 2500 ppm. That said, all CO_2 reconstructions across the Tr–J event indicate an approximate doubling of CO_2 across the Tr-J boundary that coincided with a 3–5‰ CIE (Hesselbo et al., 2002; Bacon et al., 2011), hypothesized to involve methane release as well as volcanic CO_2 (McElwain et al., 1999). The consequent global warming of ~5 °C and environmental degradation, including volcanic SO_2 pollution (Steinthorsdottir et al., 2018) and widespread wildfires (Belcher et al., 2010), led to significant turnover and extinction of both marine and terrestrial organisms.

The Jurassic period

CO_2 decreased in the Early Jurassic (Hettangian–Toarcian; 201.3–174.2 Ma) to concentrations of 500–1100 ppm based on stomatal frequency (Beerling et al., 1998; McElwain et al., 1999; Chen et al., 2001; Barbacka, 2011; Steinthorsdottir et al., 2011; Steinthorsdottir and Vajda, 2015; Pienkowski et al., 2020), phytane (Witkowski et al., 2018) and liverwort (Fletcher et al., 2008) proxies (Fig. 3). Paleosol-carbonate based CO_2 estimates suggest a higher range of ~1000 to >4000 ppm (Ghosh et al., 2005; Schaller et al., 2011; Guitierrez and Sheldon, 2012; Li et al., 2020).

Atmospheric CO_2 generally remained in the 500 to ~1300 range through the Jurassic with the exception of the Toarcian Oceanic Anoxic Event (TOAE, ~183 Ma), a major perturbation of the global carbon cycle that extended 100 s of 1000s of years and led to major changes in ocean and climate conditions. The TOAE is hypothesized to have been caused by the release of thermogenic methane owing to the intrusion of Karoo-Ferrar magma into Gondwanan coal (McElwain et al., 2005; Jenkyns, 2010). Stomatal density estimates show an initial drawdown of CO_2, followed by an abrupt transient increase of >1300 ppm, leading briefly to CO_2 of >2000 ppm (McElwain et al., 2005), against background levels of ~1000 ppm (Zhou et al., 2020). A Toarcian transient rise in CO_2 of similar magnitude and from background levels of ~1000–1300 ppm is also archived in paleosol carbonates (Li et al., 2020). Post-Toarcian OAE (174.1 to ~145 Ma) CO_2 (~1000–1300 ppm) may not have returned to pre-event concentrations (McElwain, 1998; Beerling et al., 1998; Chen et al., 2001; Beerling and Royer, 2002; Retallack, 2009; Yan et al., 2009; Wu et al., 2016).

The Cretaceous period

The proxy-derived trend in CO_2 for the Cretaceous Period (145–66 Ma), based on stomatal frequency, leaf-gas exchange, land plant $\delta^{13}C$, liverwort, phytane, and paleosol-carbonate proxies, is of rising concentrations from intermediate background levels (~500–1000 ppm) of the Jurassic to peak values in the mid-Cretaceous (~120–95 Ma; up to >2000 ppm) before declining to concentrations of mostly <1000 ppm a few million years prior to the close of the Cretaceous (Fig. 3). Overall, CO_2 estimates derived from stomatal proxies (small and larger gray squares on Fig. 3) yield overlapping to up to 50% higher values than those of the curated data (color symbols) derived using the phytane, liverwort, leaf-gas exchange, and stomatal frequency proxies. In contrast, CO_2 estimates based on the land plant $\delta^{13}C$ for this interval (gray triangles) are markedly lower (~100–400 ppm) than those indicated by all other proxy estimates, whereas CO_2 derived using the paleosol-carbonate proxy (gray circles; Nordt et al., 2003; Ghosh et al., 2005; Leier et al., 2009; Lee II., 1999; Lee II. and Hisada, 1999; Mortazavi et al., 2013; Li et al., 2014; Suarez et al., 2021) define a much larger range than the curated data (color symbols on Fig. 3).

The curated data suggest moderate CO_2 (500–800 ppm) in the very earliest Cretaceous (Fig. 3; Fletcher et al., 2008; Witkowski et al., 2018) and support transiently lowered temperatures across the Jurassic–Cretaceous boundary independently inferred from organic matter carbon isotope records (e.g. Price et al., 2016). Moreover, stomatal frequency- and paleosol carbonate-based estimates generally indicate moderately low CO_2 (<300 to ~1000 ppm, with a subset of paleosol carbonate-based values up to 2500 ppm) in the Early Cretaceous (Berriasian through Hauterivian; 145–130 Ma) (Jing and Banian, 2018; Robinson et al., 2002; Hong and Lee, 2012; Huang et al., 2012; Li et al., 2016). Low- to moderate-global surface temperatures are consistent with overall cooling in the first half of the Early Cretaceous. CO_2 likely increased through the second half of the Early Cretaceous (Hauterian-Albian (~132.6–100.5 Ma) with stomatal frequency-based CO_2 of ~600–1500 ppm (Haworth et al., 2005; Chen et al., 2001; Sun et al., 2007; Passalia, 2009; Jing and Banian, 2018) and paleosol carbonate-based estimates of 300–1300 ppm (Hong and Lee, 2012) and up to 2000 ppm (Li et al., 2014).

Several Oceanic Anoxic Events (OAEs) were superimposed on the overall elevated CO_2 of the Cretaceous Period, with the most notable of these events being OAE1a in the early Aptian (~120 Ma) and OAE2 at the Cenomanian-Turonian boundary (~94 Ma) (Arthur et al., 1988; Turgeon and Creaser, 2008; Jenkyns, 2010; Huber et al., 2018). It has long been considered that the burial of large amounts of carbon led to reduced CO_2 during these events indicated by positive carbon isotope excursions, and transiently lowered temperatures globally (Arthur et al., 1988; Li et al., 2014; Huber et al., 2018). For OAE1a (120 Ma), paleosol carbonate

proxies indicate an initial relatively rapid rise in CO_2 from background values of ~800 to up to ~1300 ppm and a subsequent longer-term decline in CO_2 concentrations to ~500 ppm by the end of the Albian (Ludvigson et al., 2015). Moderate background CO_2 (600–800 ppm) by the close of the Early Cretaceous (~100 Ma) is indicated by pedogenic carbonate (Ludvigson et al., 2015) and stomatal frequency (Du et al., 2016) proxies, supporting an independently inferred decrease in temperatures for this interval (Huber et al., 2018).

Higher-resolution leaf fossil proxy-derived CO_2 records exist for two subsequent OAE events. For the mid-Cretaceous OAE1d, which marks the Albian-Cenomanian boundary and the end of the Early Cretaceous (100.5 Ma), stomatal frequency- and leaf-gas exchange-based estimates indicate background values of 500–600 ppm and a CO_2 peak of ~840 ppm towards the end of the event (Richey et al., 2018). For OAE2 that marks the Cenomanian-Turonian boundary (93.9 Ma), stomatal frequency-based estimates indicate that CO_2 increased from background values of ~370 ppm to ~500 ppm (+400/−180 ppm) multiple times before decreasing by up to 26% by the end of the event (Barclay et al., 2010). Both OAE records document a complex relationship to the well-documented CIEs including defining a lag between the $\delta^{13}C$ excursion and the CO_2 increase (Richey et al., 2018). Relevant to advancing the science of paleo-CO_2 reconstruction, both OAE1d and OAE2 records used leaf fossil cuticle fragments of Lauraceae, an angiosperm, to reconstruct paleo-CO_2. The relative trends in CO_2 are likely robust, but for both OAE records, the significantly lower background and maximum CO_2 estimates relative to other stomatal CO_2 reconstructions built using Ginkgoales and Coniferales fossils most probably reflects that Lauraceae (and perhaps most angiosperms) underestimate paleo-CO_2 (see e.g., Kürschner et al., 2008; Steinthorsdottir et al. 2016a, 2016b, 2019a, 2019b). For OAE1d, calibrating the rise in CO_2 using late Albian background CO_2 of 800–1000 ppm (Jing and Banian, 2018) would translate to peak values (~1100–1400 ppm) at 100.5 Ma more compatible with CO_2 estimates for OAE1a (Ludvigson et al., 2015) and post-OAE1d CO_2 more on par with stomatal frequency-based CO_2 estimates of ~1000 ppm made using gymnosperms (Mays et al., 2015, Ginkgoales; Du et al., 2016, Coniferales). By the close of the Early Cretaceous (latest Albian), both leaf fossil- (Richey et al., 2018) and paleosol carbonate-based proxies indicate CO_2 of 600–500 ppm (Ludvigson et al., 2015).

By the mid-Late Cretaceous (Santonian and Campanian (86.3–72.1 Ma), stomatal frequency proxies indicate a decline in CO_2 from peak concentrations of ≥1000 ppm and possibly 2800 ppm of the mid-Cretaceous (Cenomanian and Turonian) to ~600–800 ppm (Quan et al., 2009; Wan et al., 2011). This trend (Fig. 3) is similarly suggested by paleosol-carbonate proxies, albeit at overall higher CO_2 concentrations (from 1400/1600 to ~500 ppm, Hong and Lee, 2012; 1800/2800 to 1100/1900 ppm, Ghosh et al., 2005; 1200–780 ppm, Nordt et al., 2002; ~2500–1000 ppm, Zhang et al., 2018). Stomatal-based CO_2 concentrations of ~550 of 600 ppm (see section below) for the final stage of the Cretaceous (Maastrichtian, 72.1—66 Ma) indicate that CO_2 continued to decline toward the end of the Cretaceous (Beerling et al., 2002; Steinthorsdottir et al., 2016b; Milligan et al., 2019). This continued decline is further suggested by paleosol-carbonate CO_2 estimates (Andrews et al., 1995; Nordt et al., 2002, 2003; Zhang et al., 2019c) and a limited number of phytane-based estimates (Witkowski et al., 2018) and is compatible with inferred cooling for the late-Late Cretaceous (Maastrichtian (~69 Ma); Huber et al., 2018).

The Cretaceous/Paleogene (K–Pg) boundary interval

The close of the Mesozoic Era (66 Ma) archives the most recent of Earth's five major extinctions, characterized by the obliteration of the dinosaurs and loss of ~75% of all living species. Although the Chicxulub asteroid that impacted the Yucatan Peninsula was the principal driver of this mass extinction (Alvarez et al., 1980; Schulte et al., 2010; Hull et al., 2020; Morgan et al., 2022), Deccan trap volcanism, which began a few 100,000 years before, is hypothesized to have primed the ecosystems for subsequent asteroid-related negative environmental effects (Keller, 2014; Renne et al., 2015; Zhang et al., 2018). Proxy-based estimates indicate a moderate to substantial increase in CO_2 across the K–Pg boundary interval. Curated leaf gas-exchange proxy (Milligan et al., 2019; red squares on Fig. 3) and liverwort proxy (Fletcher et al., 2008; green triangles on Fig. 3) estimates indicate a ~200–500 ppm increase in CO_2 across the K–Pg boundary from latest Cretaceous background values of ~600 to ~900 ppm (e.g., Steinthorsdottir et al., 2016b). Marine boron isotope-based estimates (500 and 1900 ppm) also record a CO_2 rise in this interval but of several-fold (blue inverted triangles on Fig. 3). Paleosol carbonate-based estimates, considered of category 2 reliability (The CenCO$_2$PIP Consortium, 2023), also indicate a moderate increase in CO_2 (a few 100 ppm) across the boundary interval (Nordt et al., 2002). Notably, a high-resolution paleosol carbonate proxy record (Zhang et al., 2018) reveals a ~500 ppm rise in CO_2 immediately prior (66.4–66.3 Ma) to the K-Pg boundary, attributed to pre-boundary Deccan volcanism, followed by a transient drop in CO_2 to ~750 ppm at the K–Pg boundary. Plant fossil-based estimates further suggest low CO_2 (~400 ppm) into the earliest Paleocene (earliest Danian) (Steinthorsdottir et al., 2016b).

Estimating paleo-CO$_2$ with long-term carbon cycle models

Key principles

Over multi-million-year timescales, the concentration of CO_2 in the atmosphere is largely controlled by a handful of processes that act to transfer carbon between crustal (sediments and rocks) and surficial (atmosphere, ocean, land surfaces) reservoirs; this system is defined as the long-term carbon cycle (Fig. 4). If the rate of these processes over time can be determined, then the trajectories of atmospheric CO_2 can be quantified on geologic timescales (Fig. 4).
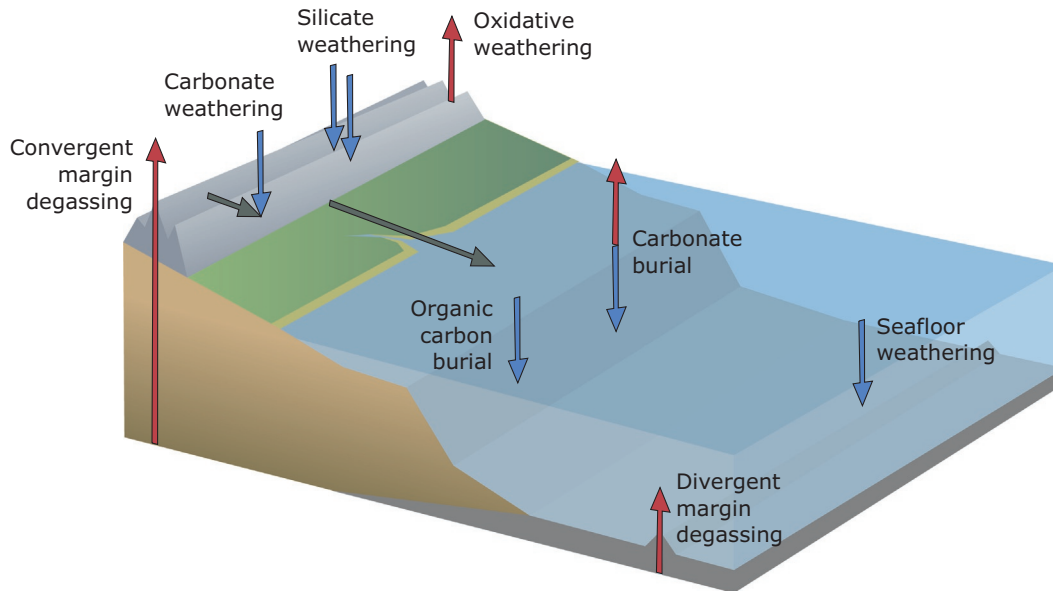
Fig. 4 The Atmosphere-Ocean-Sediment carbon cycle. Red arrows show sources to the atmosphere or ocean and blue arrows show sinks out of the atmosphere or ocean. Silicate weathering transfers 2 mol of CO_2 into solution for each mole of divalent cation (e.g. Ca) whereas carbonate weathering transfers one mole of CO_2 from the atmosphere and one from the carbonate rock. Carbonate precipitation removes one mole of carbon into sediments but releases one mole of CO_2, thus silicate weathering followed by carbonate burial is a net sink of CO_2, whereas carbonate weathering followed by carbonate burial is not (see Proxy approches to paleo-CO₂ reconstruction section). Seafloor weathering follows the same overall process as silicate weathering followed by carbonate burial, but occurs entirely locally in hydrothermal systems, so is also a net sink for CO_2. Organic carbon burial is a net sink for CO_2, whereas weathering of organic carbon in sediments, as well as degassing of carbon from either organics or carbonates, are sources.

The key processes were enumerated in 1845 by French chemist and mining engineer (Ebelmen, 1845; see also Berner and Maasch, 1996), with more modern treatments by Urey (1952), Garrels and Perry (1974), Holland (1978), Walker et al. (1981), Berner et al. (1983), Garrels and Lerman (1984), and Berner (1991, 2004). There are two main sinks for CO_2 on multi-million-year timescales. The first, mineral-based, is the 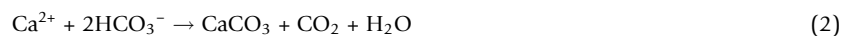formation and burial of carbonates whose ionic components (Ca^{2+}, Mg^{2+}, and HCO_3^-) derive from the weathering of Ca and Mg silicate rocks (equations 1–3).

Weathering of a generalized calcium silicate:

$$2CO_2 + H_2O + CaSiO_3 \rightarrow Ca^{2+} + 2HCO_3^- + SiO_2 \tag{1}$$
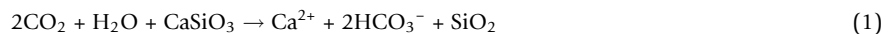
Precipitation of calcium carbonate:

$$Ca^{2+} + 2HCO_3^- \rightarrow CaCO_3 + CO_2 + H_2O \tag{2}$$

Sum of (1) and (2):

$$CO_2 + CaSiO_3 \rightarrow CaCO_3 + SiO_2 \tag{3}$$

The second major sink for CO_2 is the burial of organic matter (on land or in the ocean). This process can be conceptualized as 'geo'-photosynthesis (Eq. 4 from left-to-right).

$$CO_2 + H_2O \leftrightarrow CH_2O + O_2 \tag{4}$$

Both of these burial processes physically remove carbon from the Earth's surface until, tens-to-hundreds of millions of years later, tectonic forces return the carbon to the atmosphere via volcanism or chemical weathering of carbonates and oxidation of organic-rich rocks and sediments. (Eq. 4 from right-to-left: 'geo'-respiration).

The processes that control the long-term evolution of CO_2 are distinct from their short-term control. Most noticeably, the more familiar short-term carbon cycle ($< 10^3$ year), which involves the transfer of carbon within the surface Earth system (e.g., photosynthesis, size of the terrestrial biosphere, and the efficiency of the oceanic biological pump), is not directly relevant to the long-term carbon cycle and its multi-million-year control of atmospheric CO_2. This is because any large change in the size of these surface reservoirs (e.g., soil, marine inorganic carbon) cannot be sustained over geologically relevant timescales and can be assumed to be in quasi-steady state (Berner, 2004). For example, a sustained increase in marine productivity would deplete nutrient supply in the global ocean and become self-limiting long before millions of years of carbon burial could occur. As a result, the short-term carbon cycle dominates the control of atmospheric CO_2 over timescales of approximately $\leq 10^4$ year and the long-term carbon cycle for timescales of $\geq 10^5$ years.

Key models

Berner et al. (1983) applied these key principles to quantify multi-million-year patterns in CO_2 concentration. Berner and colleagues subsequently expanded and refined their original studies into the GEOCARB family of models (after GEOlogical CARBon; Berner, 1991, 1994; Berner and Kothavala, 2001; Berner, 2004, 2006a, 2006b, 2008, 2009; Royer et al., 2014; Krause et al., 2018; Mills et al., 2023). In these models, inputs of CO_2 to the surface system through volcanism are controlled by reconstructions of global tectonic degassing (typically related to seafloor spreading rates), and weathering inputs tend to rely on a simple approximation of global average surface temperature and global runoff rates. Burial of carbonates is related to the weathering inputs of Ca and Mg cations. The framework for computing organic carbon burial is an isotopic mass balance, where the masses and stable isotopic compositions of carbon in the surface Earth system at a given time in the past are related to the flux and isotopic values of carbon moving into and out of the system (Berner, 2004). Tracking C isotopes is helpful because many of the major reservoirs have distinct isotopic compositions, and photosynthesis drives isotopic fractionation. A sulfur isotope mass balance is also used in the more recent GEOCARBSULF models and is primarily useful for constraining atmospheric O_2 variations driven by burial and weathering of reduced sulfur species (e.g., pyrite), so is therefore not emphasized here.

Alternatively, the COPSE (after Carbon, Oxygen, Phosphorus, Sulfur and Evolution; Bergman et al., 2004; Lenton et al., 2018) and MAGic (after Mackenzie, Arvidson, Guidry interactive cycles; Arvidson et al., 2006) models do not use carbon and sulfur isotopes as inputs, but instead compute burial fluxes of pyrite and organic carbon via independent estimates of biological productivity. Estimates of CO_2 with these models tend to be less constrained, but a key advantage is that they simulate $\delta^{13}C$ and $\delta^{34}S$, which can then be compared to $\delta^{13}C$ and $\delta^{34}S$ records measured in mineral and fossil organic archives. This provides a strong iterative framework for better understanding the underlying controls of atmospheric CO_2, but has less utility in providing a 'best guess' prediction for ancient CO_2 levels. The GEOCARBSULFOR model splits the difference, using $\delta^{13}C$ as an input but not $\delta^{34}S$ (Krause et al., 2018).

Key updates

Royer et al. (2014) identified two areas in the GEOCARBSULF model that contribute the most uncertainty to estimated CO_2: (1) climate sensitivity and (2) the temperature-dependence of silicate weathering reactions in the absence of a plant biosphere in the earlier Phanerozoic (e.g., Berner, 1997; Lenton et al., 2012; Quirk et al., 2015). Global 'General Circulation' physical climate models (GCMs) are typically used to inform input decisions about climate sensitivity. Most of these climate models do not incorporate slower feedbacks (e.g., dynamics of continental ice sheets), which is a problem for long-term carbon cycle models that integrate over millions of years. Importantly, it is well established that a climate sensitivity that includes both fast and slow feedbacks ("Earth System Sensitivity"—ESS) is typically higher than a fast-feedback-only climate sensitivity (Hansen et al., 2008; Lunt et al., 2010; Rohling et al., 2012; Royer, 2016; The Cenozoic CO_2 Proxy Integration Project, 2023). GEOCARB and GEOCARB-style models can be inverted to solve for the value of climate sensitivity that minimizes the misfits to CO_2 proxy data; these analyses also support elevated Earth System Sensitivities, particularly during glacial periods (Royer et al., 2007; Park and Royer, 2011; Krissansen-Totton and Catling, 2017; Wong et al., 2021). As such, most recent implementations of long-term carbon cycle models adopt higher values of climate sensitivity (e.g., Mills et al., 2019; Marcilly et al., 2021).

In the original GEOCARB model (publications up to Berner, 2008), the factors controlling chemical weathering (temperature, soil moisture, vegetation type, topography, etc.) were considered at the global scale; that is, zero-dimensional and not spatially resolved—a single value for the entire Earth surface. This is problematic: for example, relief (e.g., mountain building) is expected to increase chemical weathering via faster exhumation of fresh minerals, but only if there is sufficient soil moisture, whereas chemical weathering in low-relief regions mantled by thick, mature soil profiles is considerably dampened (Brantley et al., 2023). There is a clear need to couple spatially-resolved weathering and climate models to long-term carbon cycle models (see Goddéris et al., 2023 for a history on this topic); one example of this approach is the GEOCLIM model (after GEOlogical timescales CLIMate; Donnadieu et al., 2004, 2006), which dynamically computes a steady state long-term climate for a given period of Earth history based on a spatial weathering module and outputs of a coarse-resolution GCM. To incorporate this approach into GEOCARBSULF, Royer et al. (2014) used spatially-resolved estimates of runoff and mean temperature of land surfaces undergoing chemical weathering from 22 simulations of GEOCLIM spanning the Phanerozoic (Goddéris et al., 2012) as inputs to drive GEOCARB (see https://doi.org/10.6084/m9.figshare.902207 for R code to run this GEOCARB model); Marcilly et al. (2021) later updated these two inputs based on improved paleogeographic reconstructions (but using an approximation to drive climate rather than a CGM) and applied them to GEOCARB. In a time-specific application, Richey et al. (2020) used the GEOCLIM model to resolve a late Paleozoic climate paradox defined by a protracted period (10 Myr) of very low CO_2 (<300 ppm) in the earliest Permian inferred from proxies. The paradigm arises given that the CO_2 nadir postdates the period of peak silicate weathering rates of the Himalayan-scale highlands of supercontinent Pangaea and is contemporaneous with pantropical aridification and onset of geographically widespread magmatism, both drivers of increased atmospheric CO_2. Modeled steady state CO_2 estimates for the 40-Myr period that account for spatial variability of mafic vs. felsic silicate weathering, compare well with the CO_2 proxy estimates and align with the GEOCARBSULFOR values for this period (Mills et al., 2023) when combined with the weathering and degassing inputs from Marcilly et al. (2021) (Fig. 5c).
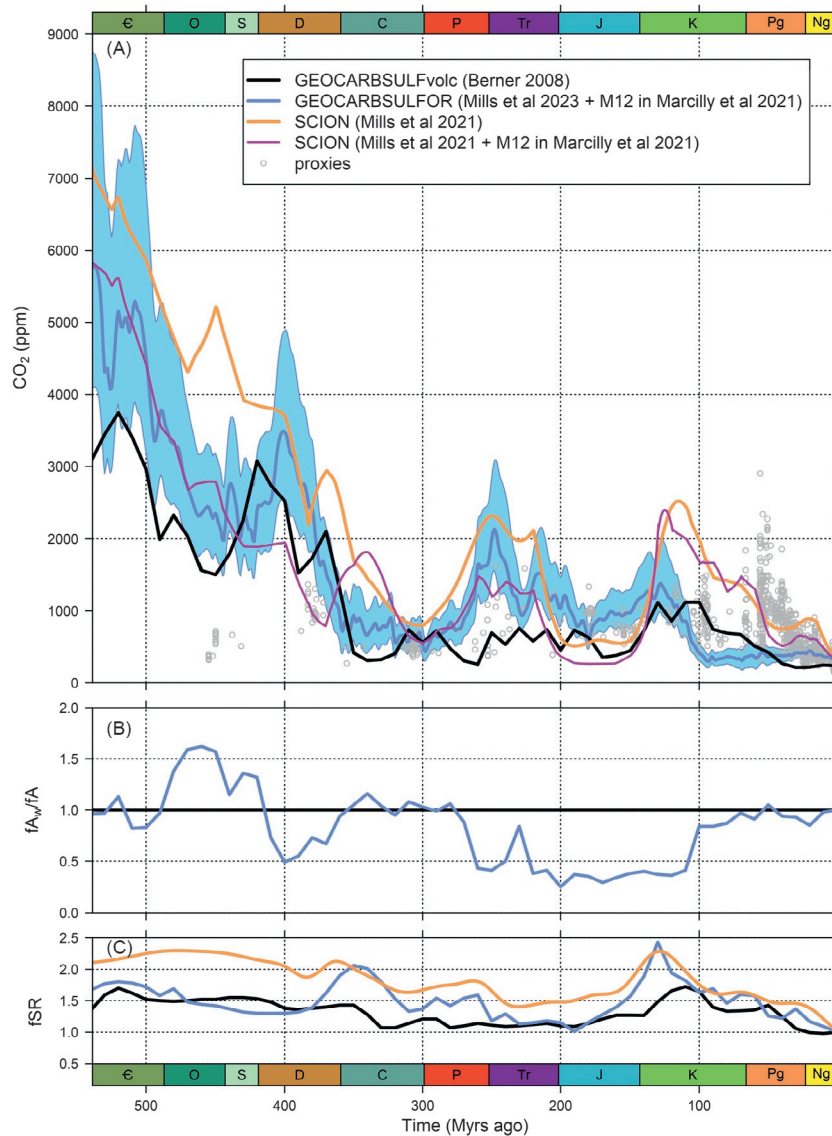
Fig. 5 Key changes to long-term carbon cycle models in the last ten years. (A) Parameterization of the fraction of land area undergoing chemical weathering, scaled to the present-day (fA_W/fA). Royer et al. (2014) introduced this factor; earlier versions have an assumed time-invariant value of 1 (black line). (B) Parameterization of tectonic degassing, scaled to the present-day (fSR). (C) Estimates of CO_2. GEOCARBSULFvolc is the version of the GEOCARB model (Berner, 2006b, 2008) presented in the last Treatise chapter on atmospheric CO_2 and O_2 (Royer, 2014). GEOCARBSULFOR (Krause et al., 2018) is the latest version of the GEOCARB model. Here we combine the simulation presented in Mills et al. (2023) with the weathering and degassing inputs of "M12" presented in Marcilly et al. (2021) (blue line; blue envelope captures 95% of the 5000 simulations). The SCION model (Mills et al., 2021), which couples COPSE with GEOCLIM, is shown in orange, whereas the SCION model with the weathering and degassing inputs of M12 (Marcilly et al., 2021) is shown in pink. The CO_2 proxy estimates shown as gray open circles are the subset that, at present, does not require any revision (identical to the colored symbols in Fig. 3).

There is a strong trajectory in long-term carbon cycle modeling towards a spatially-explicit treatment of chemical weathering. Indeed, Mills et al. (2021) recently integrated the GEOCLIM climate module with COPSE in a coupled model called SCION (Spatial Continuous IntegratiON) which is able to dynamically integrate the 3D steady state climate over Phanerozoic timescales, rather than being restricted to 'snapshots' for a given continental configuration. This still does not represent a complete coupling between climate and the long-term carbon cycle, because the 3D climate is an interpolated steady state taken from a set of climate model runs, rather than the climate model running alongside the carbon cycle model. Given that even simple GCM typically take days to weeks to run simulations of ∼10,000 years, it is unlikely that a true dynamical coupling over geological time will be possible without a major step change in computational resources or techniques. However, with a range of more detailed systematic global climate model simulations becoming available, for example the 109 simulations from Valdes et al. (2021; one per Phanerozoic stage and currently being run to include water oxygen isotopes), steady state couplings like those employed in GEOCLIM and SCION could significantly improve in the future.

Another aspect of long-term carbon cycle modeling with rapid development in the last decade is tectonic degassing (e.g., volcanism). Originally, degassing was scaled from reconstructed seafloor spreading rates (and, for times older than the oldest intact seafloor, spreading was inferred from reconstructions of sea level—representing changing ridge volumes). There are now many models for the Phanerozoic patterns of rifting (including continental rifts), subduction (and its interaction with carbonate platforms), and arc volcanism, which all contribute to tectonic degassing (e.g., Lee et al., 2013; McKenzie et al., 2016; Pall et al., 2018; Domeier and Torsvik, 2019; Macdonald et al., 2019; Müller et al., 2022). These revised inputs are now becoming standard in long-term carbon cycle model simulations of CO_2 (e.g., van der Meer et al., 2014; Brune et al., 2017; Marcilly et al., 2021; Mills et al., 2021).

Key patterns

Fig. 5A compares two newer CO_2 simulations against the GEOCARBSULFvolc benchmark (Berner, 2006b, 2008) presented in the 2014 Treatise (Royer, 2014), all compared to proxy-estimates of paleo-CO_2. The GEOCARBSULFOR (Krause et al., 2018) simulation is based on the latest version (https://github.com/Alexjkrause; accessed June 2023) presented in Mills et al. (2023) combined with the updated weathering and degassing inputs associated with "Model 12" (M12) from Marcilly et al. (2021). In this model, CO_2 during the Permian-to-Jurassic is higher than in Berner (2006b, 2008) because the revised fraction of land area undergoing chemical weathering is lower (fA_w/fA; Fig. 5B) and the revised rate of tectonic degassing is higher (fSR; Fig. 5C). These higher CO_2 estimates are more in keeping with the proxy evidence (Fig. 5A), largely erasing a previous model-proxy mismatch.

The SCION simulation (Mills et al., 2021), based on the latest version V1.1.6 (https://github.com/bjwmills), predicts higher CO_2 than the GEOCARB simulations for much of the Phanerozoic. Up until 200 Myr ago, this difference is largely due to higher prescribed tectonic degassing (Fig. 5C), which is based on reconstructed slab fluxes and subduction zone lengths from plate models. Indeed, when SCION is run with the degassing input from M12 of Marcilly et al. (2021) (based on the age of zircons, which are produced in arc environments), CO_2 during this interval is much more similar to GEOCARBSULFOR also run with M12 of Marcilly et al. (2021) (purple vs. blue lines in Fig. 5A).

SCION also predicts higher CO_2 from the Cretaceous to present-day when compared to the GEOCARB models. This cannot be explained by a difference in degassing (Fig. 5C) because the two degassing records are very similar over this time, due in part to much better preservation of oceanic crust over the last 200 Myr which facilitates plate reconstruction. Indeed, the modified SCION run is nearly identical to its default run during this time (purple vs. orange lines in Fig. 5A). Instead, the difference is related to a weaker chemical weathering feedback in SCION (vs. GEOCARB) during the Cretaceous and Paleogene. This is confirmed when early versions of SCION are compared to the COPSE model over this timeframe—in which the only differences between the models were the climate module (Mills et al., 2021). Because SCION spatially resolves chemical weathering through its 'offline' coupling with GCM, its results during this period are generally taken to be more robust. That said, predictions of the organic carbon cycle are still likely to be more realistic in GEOCARB models due to the isotope mass balance technique.

Clearly, spatial consideration of chemical weathering is an important consideration because—at least for the Paleogene and Neogene—SCION is much more consistent with the CO_2 proxies (Fig. 5A); indeed, low Cenozoic CO_2 estimates from recent COPSE and GEOCARB models are a well-studied but still chronic problem in long-term carbon cycle research (e.g., Park and Royer, 2011; van der Meer et al., 2014; Krause et al., 2018; Lenton et al., 2018; Mills et al., 2019; Marcilly et al., 2021). Brune et al. (2017) previously addressed this problem by arguing for elevated degassing via continental rifting during the mid-Cenozoic. When they ran GEOCARB with a rifting control on CO_2 emissions, the mismatch to the proxies disappeared. However, continental rifting is not currently thought to be the dominant process responsible for tectonic CO_2 outgassing—the rifting record of Brune et al. (2017) is incorporated into global CO_2 emissions in the SCION model (orange line, Fig. 5A), and along with altered chemical weathering intensity, helps explain some of the previous model-data mismatch over the Cenozoic.

Another important timeframe where models fail to replicate CO_2 proxies is the Ordovician-Silurian. There are few proxies from this time, but they tend to agree on relatively low values around 500 ppm, whereas the SCION and GEOCARB family of models typically predict over 2000 ppm. It is likely that the proxies are closer to the truth than the models here, because it is known that the mid-late Ordovician experienced ice sheet advance to paleolatitudes approximately equal to the Pleistocene, implying a similar or indeed lower surface temperature than the preindustrial—although because of the lower solar flux in the Paleozoic (e.g. Kasting, 1989) we would still expect CO_2 levels to be significantly higher than during the Pleistocene. Nevertheless, replicating low Ordovician surface temperature in physical climate models requires less than 1000 ppm in the Fast Ocean and Atmosphere Model (FOAM; Goddéris et al., 2014), and approximately the same value in the HadCM3BL climate model (Valdes et al., 2021; 2 °C above pre-Industrial at ~1600 ppm).

There have been several attempts to reproduce lower CO_2 concentrations in the earlier Paleozoic in carbon cycle models. Lenton et al. (2012) suggested that early nonvascular plants, which colonized the land during the Ordovician period, had a substantial impact on chemical weathering and organic carbon burial, and therefore led to transient lower steady-state CO_2 concentrations, which depended on an episodic release of the nutrient phosphorus as plants exhausted weatherable terranes. This idea also potentially explains the large positive carbon isotope excursions that appear to accompany cooling in the Ordovician—as these could reflect increased burial of isotopically-light organic carbon when phosphorus is more readily available. An alternative explanation for these isotope excursions and CO_2 drawdown is that bioavailable phosphorus was instead delivered to the ocean through a large period of explosive volcanism known to have occurred during the later Ordovician (Longman et al., 2021), and was efficiently recycled to marine photosynthesizers during periods of marine anoxia associated with the late Ordovician extinction

(Qiu et al., 2022). Further hypotheses for later Ordovician cooling focus on the exposure of weatherable lithologies in the humid tropics during this time—potentially volcanic arcs (Young et al., 2009) and/or arc-continent collisions which expose more reactive silicate material (Macdonald et al., 2019). To date, there has not been a quantitative comparison of these ideas within a numerical framework. None are well-represented within the plotted GEOCARB or SCION models.

Next steps in carbon cycle modeling

The mode towards spatial representation of climate and weathering processes has improved the data-model mismatch over the Cretaceous and Cenozoic. There is still work to do with these models in better representing and assessing potential drivers of Paleozoic changes in CO_2 levels, but this approach is also still in its infancy, and general advancements may also help to resolve data-model challenges throughout the Phanerozoic.

Improving spatial and temporal resolution of climate model data

The spatially-resolved long-term carbon cycle models GEOCLIM and SCION both use steady state outputs of the climate model FOAM (Jacob, 1997; Donnadieu et al., 2006) to parameterize their spatial surface processes. But FOAM is a relatively old and coarse-resolution model (48×40 grid boxes, or an average of $7.5^0 \times 4.5^0$ long/lat per grid box). Much higher resolution climate models are now routinely used for paleoclimate simulation, for example HadCM3L (96×73 boxes or $3.75^0 \times 2.5^0$; Valdes et al., 2021) or CESM (288×192 boxes, or $1.25^0 \times 0.94^0$; e.g., Macarewich et al. 2021; Matthaeus et al., 2023). The use of an older and less computationally-expensive model is a result of the large number of simulations required to build an accurate climate emulator for use with the carbon cycle model—i.e. a data structure in which many CO_2 levels and time points are sampled and one can therefore input a time period and CO_2 level and retrieve an instantaneous estimate of spatially-resolved temperature and hydrology. This computational expense also limits the number of time points that can be run in the climate model: the current FOAM simulations are performed every 20–40 Myrs, and thus struggle to represent changes in continental configuration on shorter timescales. In the coming years, larger data structures of model runs (e.g. many CO_2 levels and many time points) will likely become available for more modern climate models, and will undoubtedly improve the representation of surface processes in models like GEOCLIM and SCION, which may help resolve model-data mismatch.

Improving representation of non-silicate weathering processes

Silicate weathering is a major focus of long-term carbon cycle models, as this is the major abiotic sink for CO_2 over long timescales. But other continental weathering processes are also important for controlling atmospheric CO_2 concentration. While current models all use some representation of the weathering of organic carbon, sulfides and sulfates, the recent advances in spatially-resolved representation have not yet been extended to these species. Erosion can supply phases other than silicate for weathering leading to weathering-induced CO_2 emissions that can release as much CO_2 as volcanoes (Hilton, 2023). Oxidative weathering of organic carbon is a major source of CO_2, and also displays significant lithological and erosion dependence which may impact the long-term carbon cycle (Hilton and West, 2020). Weathering of sulfides has been shown to impact the long-term carbon cycle through production of sulfuric acid that dissolves carbonate rocks (Torres et al., 2014), and while this has been incorporated in a simple manner into some long-term carbon cycle models with minimal effect (Mills et al., 2014), more complete treatments of continental processes and marine chemistry may alter how this process impacts CO_2 levels (Maffre et al., 2021). Sulfate (e.g., gypsum) weathering is also likely to impact the long-term carbon cycle through delivery of calcium, which alters $CaCO_3$ solubility in seawater and ultimately may change the burial rate of carbonate minerals (Shields and Mills, 2021).

Simplified ocean chemistry

Current long-term carbon cycle models tend to use an extremely simple representation of marine chemistry which assumes alkalinity balance, and therefore equates total deposition of carbonate minerals to the terrestrial inputs of the major divalent cations (Ca, Mg) and bicarbonate ions (HCO_3^-). In reality, carbonate deposition is controlled by the availability of the Ca^{2+} and CO_3^{2-} ions in seawater, and thus changes to this balance independent of silicate and carbonate weathering (e.g. through addition or removal of calcium, or changes to temperature or pH) might lead to different model predictions for variations in atmospheric CO_2 concentration.

Reverse weathering

Reverse weathering is the process by which weathering products combine to form marine clays rather than carbonate minerals. With high levels of reverse weathering, the silicate weathering feedback would be effectively nullified and atmospheric CO_2 levels could rise. It has been suggested that high-silica oceans, in the time before siliceous organisms evolved, resulted in the generally high CO_2 levels of the Precambrian through increased reverse weathering (Isson and Planavsky, 2018). High levels of reverse weathering—due to extinction of many siliceous organisms at the Permian-Triassic Mass Extinction—have also been suggested as a driver of very high Early Triassic CO_2 levels (Cao et al., 2022; Isson et al., 2022). Unfortunately, there is no clear proxy record of reverse weathering and its contribution to the present-day carbon cycle may be minimal (Isson and Planavsky, 2018), making the process extremely difficult to model and assess accurately at the global scale. Nevertheless, it is not incorporated into any current long-term carbon cycle models.

Terrestrial lithology

Current spatially-resolved long-term carbon cycle models tend to assume a homogeneous global continental lithology, whereas lithology is extremely important for present day silicate (and other major) weathering rates. As discussed in the Current status of paleo-CO$_2$ reconstructions section, more reactive mafic silicates in arcs and suture zones are known to weather more rapidly, and when considered in spatially-resolved modeling studies have been shown to strongly impact steady state CO$_2$ (Richey et al., 2020). Future models should include these into their continental process calculations. This 'volcanic' weathering has been considered in GEOCARB models for many years (e.g. Berner, 2008), but only at the global scale, based on global availability of volcanic rock. But it is the local coincidence of volcanic terranes with vigorous hydrology and high temperatures which should lead to locally-enhanced weathering rates during some periods, whereas high-latitude volcanic provinces like the Siberian Traps probably contribute very little to global silicate weathering.

Terrestrial vegetation

As discussed in Section 9.8.3.3, the effect of vegetation on enhancing silicate weathering has been incorporated into the GEOCARB models since their inception, but at the global scale. Again, this effect is likely to be pronounced in some areas and restricted in others, which may become particularly uncertain where high erosion rates allow for rapid weathering but restrict the habitability for plants. Recent investigations into the spatially-resolved effects of land plant colonization reveal complex relationships that are not included in current long-term carbon cycle models (Maffre et al., 2021; Matthaeus et al., 2021, 2023).

Combining isotope mass balance with spatially-resolved surface processes

In the current literature, the GEOCARB models are better at reconstructing organic carbon fluxes because they use isotope mass balance calculations to infer these rates from the geological record of carbon isotopes. However, spatial models like SCION are arguably better at representing the inorganic carbon cycle because of their more detailed treatment of silicate weathering. Thus, our best estimates of paleo-CO$_2$ may come from combining the spatially-resolved models with the isotope mass balance approach for their organic carbon fluxes.

Summary and future directions for paleo-CO$_2$ reconstruction

The record of paleo-CO$_2$ and its influence on climate, ecosystems and surface processes is integral to understanding interactions in the Earth System. How atmospheric CO$_2$ has evolved over time is also key to understanding how surface processes and ecosystems may respond to and function under future high CO$_2$ concentrations as paleo-CO$_2$ reconstructions are the only observational source of such information. In this review, we discussed the commonly used marine and terrestrial proxies available for paleo-CO$_2$ reconstruction, addressing the environmental and/or physiologic processes that mechanistically link each proxy to CO$_2$ and the challenges in their application as well as the opportunities for proxy advancements. We presented a Phanerozoic compilation of all published paleo-CO$_2$ estimates ($n = 4077$) that illustrates broad patterns in paleo-CO$_2$ that studies indicate are robust on the first order. The same compilation, however, reveals considerable scatter in CO$_2$ estimates for many geologic intervals. These broad ranges in values reflect inconsistencies between proxy estimates and the paucity of well-constrained and systematically defined uncertainties for many. These limitations in turn, largely reflect uncertainty about how environmental and ecological processes and conditions affect the CO$_2$ proxy signals. That said, considerable advancements in deep-time proxy validation and application and development and refinements of modeling approaches have been made by the paleo-CO$_2$ community over the past decade with ongoing efforts targeting further needs.

We highlighted a recently published, high-fidelity CO$_2$ record for the Cenozoic (The CenCO$_2$PIP Consortium, 2023) that substantially improves our understanding of the evolution of CO$_2$ over the past 66 Myr and sets the benchmark for future paleo-CO$_2$ reconstructions. A second phase of the international CO$_2$ Proxy Integration Project, the Phanerozoic CO$_2$PIP, is currently underway with the primary goals to improve the precision and accuracy of paleo-CO$_2$ estimates for the pre-Cenozoic and to build a statistically robust multi-proxy atmospheric CO$_2$ record for the Phanerozoic. This ongoing effort builds on the success of the CenCO$_2$PIP Consortium, continuing to develop the standardized paleo-CO$_2$ proxy data repository that includes all metadata and updated chronology and meets FAIR (findable, accessible, interoperable, reusable) data standards. The Consortium is modernizing published pre-Cenozoic CO$_2$ proxy records based on modern proxy theory, focusing on paleosol- and fossil leaf-based CO$_2$ proxies. Quantified representations (forward proxy system models) of the conditions and processes that govern the CO$_2$ signal are being built by the Consortium for commonly used proxies to advance our understanding of proxy sensitivities to individual controls that affect the accuracy and precision of CO$_2$ estimates. Ultimately, statistical integration of the new proxy models with the vetted and modernized proxy data using inversion analysis will produce quantitative, data-driven CO$_2$ reconstructions for individual records and will generate a robust, quantitative reconstruction of atmospheric CO$_2$ concentrations through the Phanerozoic.

Considerable progress in improving the accuracy and precision of existing and future records is anticipated. That said, much about how the CO$_2$-climate interplay within the carbon cycle shapes the Earth system, as well as the complex and reciprocal impacts on and responses of the lithosphere, hydrosphere and atmosphere, can be deciphered from the existing CO$_2$ record. It is in this context that we offered in this review an overview of the current understanding of pre-Cenozoic CO$_2$ evolution in an Earth system perspective. The CO$_2$PIP Consortium invites paleo-CO$_2$ experts to engage in this modernization process by contributing

their paleo-CO$_2$ records and associated metadata to the community project 'archive' (paleo-co2.org) and to join the vetting and updating of records when they no longer conform to the ever-evolving understanding of the proxies. Proxy-specific data templates are provided on the website to facilitate new data contributions and to ensure that the compilation stays current. Analogous to the growing paleo-CO$_2$ 'archive', the vetted 'product' compilation will be updated periodically and made accessible through paleo-co2.org, NCDC and Zenodo.

We overviewed carbon cycle models (GEOCARB family of models, COPSE, SCION) that have been used to quantify the long-term evolution of atmospheric CO$_2$. Carbon cycle modeling has been an important approach for over three decades to reconstruct the evolution of atmospheric CO$_2$ on the multi-million-year timescale as they quantitatively represent the key processes that transfer carbon between Earth's crustal and surficial reservoirs. We discussed several key updates that target the uncertainty in modeled CO$_2$, including efforts to better constrain climate sensitivity and to spatially resolve climate, hydrologic, and lithologic factors that control chemical weathering in long-term carbon cycle models. Key patterns in recent modeling efforts were presented and discussed in the context of to what degree they improve data-model mismatches, in particular for the Cretaceous through Cenozoic. Seven areas for consideration in future carbon cycle modeling were offered ranging from improved spatial and temporal resolution of climate model data and better representation of spatially resolved surface lithologies and terrestrial vegetation, and of non-silicate weathering processes and of reverse weathering, among other targets.

Acknowledgments

References

Alvarez LW, Alvarez W, Asaro F, and Michel HV (1980) Extraterrestrial cause for the Cretaceous-Tertiary extinction. *Science* 208: 1095–1108.

Anagnostou E, John EH, Edgar KM, Foster GL, Ridgwell A, Inglis GN, Pancost RD, Lunt DJ, and Pearson PN (2016) Changing atmospheric CO$_2$ concentration was the primary driver of early Cenozoic climate. *Nature* 533: 380–384. https://doi.org/10.1038/nature17423.

Anagnostou E, John EH, Babila TL, Sexton PF, Ridgwell A, Lunt DJ, Pearson PN, Chalk TB, Pancost RD, and Foster GL (2020) Proxy evidence for state-dependence of climate sensitivity in the Eocene greenhouse. *Nature Communications* 11: 4436. https://doi.org/10.1038/s41467-020-17887-x.

Andrews JE, Tandon SK, and Dennis PF (1995) Concentration of carbon dioxide in the Late Cretaceous atmosphere. *Journal of the Geological Society of London* 152: 1–3.

Arthur MA, Dean WE, and Pratt LM (1988) Geochemical and climatic effects of increased marine organic carbon burial at the Cenomanian–Turonian boundary. *Nature* 335: 714–717.

Arvidson RS, Mackenzie FT, and Guidry M (2006) MAGic: A Phanerozoic model for the geochemical cycling of major rock-forming components. *American Journal of Science* 306: 135–190. https://doi.org/10.2475/ajs.306.3.135.

Bacon KL, Belcher CM, Hesselbo SP, and McElwain JC (2011) The Triassic–Jurassic boundary carbon-isotope excursion expressed in taxonomically identified leaf cuticles. *Palaios* 26: 461–469.

Badger MPS (2021) Alkenone isotopes show evidence of active carbon concentrating mechanisms in coccolithophores as aqueous carbon dioxide concentrations fall below 7μmol L −1. *Biogeosciences* 18: 1149–1160. https://doi.org/10.5194/bg-18-1149-2021.

Barbacka M (2011) Biodiversity and the reconstruction of Early Jurassic Flora from the Mecsek Mountains (southern Hungary). *Acta Palaeobotanica* 51: 127–179.

Barclay RS and Wing SL (2016) Improving the Ginkgo CO$_2$ barometer: Implications for the early Cenozoic atmosphere. *Earth and Planetary Science Letters* 439: 158–171.

Barclay RS, McElwain JC, and Sageman BB (2010) Carbon sequestration activated by a volcanic CO$_2$ pulse during Ocean Anoxic Event 2. *Nature Geoscience* 3: 205–208.

Beerling DJ (2002) Palaeoclimatology: CO$_2$ and the end-Triassic mass extinction. *Nature* 415: 386–387.

Beerling DJ and Royer DL (2002) Reading a CO$_2$ signal from fossil stomata. *New Phytologist* 153: 387–397.

Beerling DJ and Royer DL (2011) Convergent Cenozoic CO$_2$ history. *Nature Geoscience* 4: 418–420.

Beerling DJ, McElwain JC, and Osborne CP (1998) Stomatal responses of the 'living fossil' *Ginkgo biloba* L. to changes in atmospheric CO$_2$ concentrations. *Journal of Experimental Botany* 49: 1603–1607.

Beerling DJ, Lomax B, Royer D, Upchurch G, and Kump L (2002) An atmospheric pCO$_2$ reconstruction across the Cretaceous-Tertiary boundary from leaf megafossils. *Proceedings of the National Academy of Sciences* 99: 7836–7840.

Belcher CM, Mander L, Rein G, Jervis FX, Haworth M, Hesselbo SP, Glasspool IJ, and McElwain JC (2010) Increased fire activity at the Triassic/Jurassic boundary in Greenland due to climate-driven floral change. *Nature Geoscience* 3: 426–429.

Benton M and Twitchett RJ (2003) How to kill (almost) all life: the end-Permian extinction event. *Trends in Ecology & Evolution* 18: 358–365. https://doi.org/10.1016/S0169-5347(03)00093-4.

Bereiter B, Eggleston S, Schmitt J, Nehrbass-Ahles C, Stocker T, Fischer H, Kipfstuhl S, and Chappellaz J (2015) Revision of the EPICA Dome C CO$_2$ record from 800 to 600 kyr before present. *Geophysical Research Letters* 42: 542–549. https://doi.org/10.1002/2014GL061957.

Bergman NM, Lenton TM, and Watson AJ (2004) COPSE: A new model of biogeochemical cycling over Phanerozoic time. *American Journal of Science* 304: 397–437. https://doi.org/10.2475/ajs.304.5.397.

Berner RA (1991) A model for atmospheric CO$_2$ over Phanerozoic time. *American Journal of Science* 291: 339–376. https://doi.org/10.2475/ajs.291.4.339.

Berner RA (1994) GEOCARB II: A revised model of atmospheric CO$_2$ over Phanerozoic time. *American Journal of Science* 294: 56–91. https://doi.org/10.2475/ajs.294.1.56.

Berner RA (1997) The rise of plants ad their effect of weathering and atmospheric CO$_2$. *Science* 276(5312): 544–546.

Berner RA (2004) *The Phanerozoic Carbon Cycle: CO$_2$ and O$_2$*. New York: Oxford University Press.

Berner RA (2006a) GEOCARBSULF: A combined model for Phanerozoic atmospheric O$_2$ and CO$_2$. *Geochimica et Cosmochimica Acta* 70: 5653–5664. https://doi.org/10.1016/j.gca.2005.11.032.

Berner RA (2006b) Inclusion of the weathering of volcanic rocks in the GEOCARBSULF model. *American Journal of Science* 306: 295–302. https://doi.org/10.2475/05.2006.01.

Berner RA (2008) Addendum to "inclusion of the weathering of volcanic rocks in the GEOCARBSULF model". *American Journal of Science* 308: 100–103. https://doi.org/10.2475/01.2008.04.

Berner RA (2009) Phanerozoic atmospheric oxygen: New results using the GEOCARBSULF model. *American Journal of Science* 309: 603–606. https://doi.org/10.2475/07.2009.03.

Berner RA and Kothavala Z (2001) GEOCARB III: A revised model of atmospheric CO₂ over Phanerozoic time. *American Journal of Science* 301: 182–204. https://doi.org/10.2475/ajs.301.2.182.

Berner RA and Maasch KA (1996) Chemical weathering and controls on atmospheric O₂ and CO₂: Fundamental principles were enunciated by J.J. Ebelmen in 1845. *Geochimica et Cosmochimica Acta* 60: 1633–1637. https://doi.org/10.1016/0016-7037(96)00104-4.

Berner RA, Lasaga AC, and Garrels RM (1983) The carbonate-silicate geochemical cycle and its effect on atmospheric carbon dioxide over the past 100 million years. *American Journal of Science* 283: 641–683. https://doi.org/10.2475/ajs.283.7.641.

Bolton CT and Stoll HM (2013) Late Miocene threshold response of marine algae to carbon dioxide limitation. *Nature* 500: 558–562.

Bonis NR, Van Konijnenburg-Van Cittert JHA, and Kürschner WM (2010) Changing CO₂ conditions during the end-Triassic inferred from stomatal frequency analysis on Lepidopteris ottonis (Goeppert) Schimper and Ginkgoites taeniatus (Braun) Harris. *Palaeogeography Palaeoclimatology Palaeoecology* 295. https://doi.org/10.1016/j.palaeo.2010.05.034. 146–16.

Brantley SL, Shaughnessy A, Lebedeva MI, and Balashov VN (2023) How temperature-dependent silicate weathering acts as Earth's geological thermostat. *Science* 379: 382–389.

Breecker DO (2010) *Improving paleosol carbonate based estimates of ancient atmospheric CO2*, p. 144. Geochemical News.

Breecker DO (2013) Quantifying and understanding the uncertainty of atmospheric CO₂ concentrations determined from calcic paleosols. *Geochemistry, Geophysics, Geosystems* 14: 3210–3220. https://doi.org/10.1002/ggge.20189.

Breecker DO and Retallack GJ (2014) Refining the pedogenic carbonate atmospheric CO₂ proxy and application to Miocene CO₂. *Palaeogeography, Palaeoclimatology, Palaeoecology* 406: 1–8.

Brune S, Williams SE, and Müller RD (2017) Potential links between continental rifting, CO₂ degassing and climate change through time. *Nature Geoscience* 10: 941–946. https://doi.org/10.1038/s41561-017-0003-6.

Burkhardt S, Riebesell U, and Zondervan I (1999) Effects of growth rate, CO₂ concentration, and cell size on the stable carbon isotope fractionation in marine phytoplankton. *Geochimica et Cosmochimica Acta* 63: 3729–3741.

Caballero R and Huber M (2013) State-dependent climate sensitivity in past warm climates and its implications for future climate projections. *Proceedings of the National Academy of Sciences* 110: 14162–14167. https://doi.org/10.1073/pnas.1303365110.

Cao C, Bataille CP, Song H, Saltzman MR, and Tierney-Cramer K (2022) Persistent late Permian to Early Triassic warmth linked to enhanced reverse weathering. *Nature Geoscience* 15: 832–838.

Cerling TE (1991) Carbon dioxide in the atmosphere: Evidence from Cenozoic and Mesozoic paleosols. *American Journal of Science* 291: 377–400. https://doi.org/10.2475/ajs.291.4.377.

Cerling TE (1992) Use of carbon isotopes in paleosols as an indicator of the P(CO₂) of the paleoatmosphere. *Global Biogeochem Cycles* 6: 307–314. https://doi.org/10.1029/92GB01102.

Cerling TE (1999) Stable carbon isotopes in paleosol carbonates. In: Thiry M and Simon-Coincon R (eds.) *Palaeoweathering, Palaeosurfaces and Related Continental Deposits*, pp. 43–60. Inter. Soc. Sediment. Spec. Pub. 27, Tulsa.

Chen LQ, Li CS, Chaloner WG, Beerling DJ, Sun QS, Collinson ME, and Mitchell PL (2001) Assessing the potential for the stomatal characters of extant and fossil *Ginkgo* leaves to signal atmospheric CO₂ change. *American Journal of Botany* 88: 1309–1315.

Chen J, Montañez IP, Macarewich SI, Planavsky NJ, Zhang S, Issen TT, Zhang F, Yao L, Qi Y, Wang Y, Fan J, Anbar A, Shen S, and Wang X (2022) Marine anoxia linked to abrupt global warming during Earth's penultimate icehouse. *Proceedings of the National Academy of Sciences of the United States of America* 119. https://doi.org/10.1073/pnas.2115231119.

Cleveland DM, Nordt LC, Dworkin SI, and Atchley SC (2008) Pedogenic carbonate isotopes as evidence for extreme climatic events preceding the Triassic-Jurassic boundary: Implications for the biotic crisis? *Geological Society of America Bulletin* 120: 1408–1415. https://doi.org/10.1130/B26332.1.

Cotton JM and Sheldon ND (2013) New constraints on using paleosols to reconstruct atmospheric pCO₂. *Geological Society of America Bulletin* 124: 1411–1423.

Cox JE, Railsback LB, and Gordon EA (2001) Evidence from Catskill pedogenic carbonates for a rapid Late Devonian decrease in atmospheric carbon dioxide concentrations. *Northeastern Geology and Environmental Sciences* 23: 91–102.

Cramwinckel JM, Coxall HC, Sliwinska KK, Polling M, Harper DT, et al. (2018) A warm, stratified, and restricted Labrador Sea across the Middle Eocene and its Climatic Optimum. *Paleoceanography and Paleoclimatology* 35. https://doi.org/10.1029/2020PA003932. e2020PA003932.

Cui Y and Shubert BA (2016) Quantifying uncertainty of past pCO₂ determined from changes in C3 plant carbon isotope fractionation. *Geochimica et Cosmochimica Acta* 172: 127–138. https://doi.org/10.1016/j.gca.2015.09.032.

Dahl TW and Arens SKM (2020) The impacts of land plant evolution on Earth's climate and oxygenation state - An interdisciplinary review. *Chemical Geology* 547: 119665. https://doi.org/10.1016/j.chemgeo.2020.119665.

Demicco RV and Lowenstein TK (2019) When "evaporites" are not formed by evaporation: The role of temperature and pCO₂ on saline deposits of the Eocene Green River Formation, Colorado, USA. *Geological Society of America Bulletin* 132: 1365–1380.

Diffenbaugh NS and Barnes EA (2023) Data-driven predictions of the time remaining until critical global warming thresholds are reached. *Proceedings of the National Academy of Sciences of the United States of America* 120: e2207183120. https://doi.org/10.1073/pnas.2207183120.

Domeier M and Torsvik TH (2019) Full-plate modelling in pre-Jurassic time. *Geological Magazine* 156: 261–280. https://doi.org/10.1017/S0016756817001005.

Donnadieu Y, Goddéris Y, Ramstein G, Nédélec A, and Meert J (2004) A 'snowball Earth' climate triggered by continental break-up through changes in runoff. *Nature* 428: 303–306. https://doi.org/10.1038/nature02408.

Donnadieu Y, Goddéris Y, Pierrehumbert RT, Dromart G, Fluteau F, and Jacob R (2006) A GEOCLIM simulation of climatic and biogeochemical consequences of Pangea breakup. *Geochemistry, Geophysics, Geosystems* 7. https://doi.org/10.1029/2006GC001278. Q11019.

Driese SG and Mora CI (2002) Paleopedology and stable-isotope geochemistry of late Triassic (Carnian–Norian) paleosols, Durham sub-basin, North Carolina, U.S.A.: Implications for paleoclimate and paleoatmospheric pCO₂. In: Renaut RW and Ashley GM (eds.) *, Sedimentation in Continental Rifts, Soc. Sediment. Spec. Publ. 73*, Tulsa, pp. 207–218.

Driese SG, Mora CI, and Elick JM (2000) The paleosol record of increasing plant diversity and depth of rooting and changes in atmospheric pCO₂ in the Siluro-Devonian. In: Gastaldo RA and DiMichele WA (eds.) *Phanerozoic Terrestrial Ecosystems. Paleont. Soc. Spec. Papers 6*, pp. 47–61.

Du B, Sun B, Zhang M, Yang G, Xing L, Tang F, and Bai Y (2016) Atmospheric palaeo-CO₂ based on the carbon isotope and stomatal data of Cheirolepidiaceae from the Lower Cretaceous of the Jiuquan Basin, Gansu Province. *Cretaceous Research* 62: 142–153. https://doi.org/10.1016/j.cretres.2015.07.020.

Ebelmen JJ (1845) Sur les produits de la décomposition des especes minérales de la famille des silicates. *Annales des Mines* 7: 3–66.

Ekart DD, Cerling TE, Montañez IP, and Tabor NJ (1999) A 400 million year carbon isotope record of pedogenic carbonate: Implications for paleoatmospheric carbon dioxide. *American Journal of Science* 299: 805–827.

Eugster HP (1966) Sodium carbonate-bicarbonate minerals as indicators of PCO₂. *Journal of Geophysical Research* 71: 3369–3377.

Fielding CR, Frank TD, and Isbell JL (2008) *Resolving the Late Paleozoic ice age in time and space*. Geol. Soc. Amer. Spec. Paper 441, Boulder, 354 p, https://doi.org/10.1130/SPE441.

Fletcher BJ, Brentnall SJ, Quick WP, and Beerling DJ (2006) BRYOCARB: A process-based model of thallose liverwort carbon isotope fractionation in response to CO₂, O₂, light and temperature. *Geochimica et Cosmochimica Acta* 70: 5676–5691.

Fletcher BJ, Brentnall SJ, Anderson CW, Berner RA, and Beerling DJ (2008) Atmospheric carbon dioxide linked with Mesozoic and early Cenozoic climate change. *Nature Geoscience* 1: 43–48. https://doi.org/10.1038/ngeo.2007.29.

Foster GL, Royer DL, and Lunt DL (2017) Future climate forcing potentially without precedent in the last 420 million years. *Nature Communications* 8: 14845.

Franks PJ, Royer DL, Beerling DJ, Van de Water PK, Cantrill DJ, Barbour MM, and Berry JA (2014) New constraints on atmospheric CO₂ concentration for the Phanerozoic. *Geophysical Research Letters* 41: 4685–4694. https://doi.org/10.1002/2014gl060457.

Freeman KH and Hayes JM (1992) Fractionation of carbon isotopes by phytoplankton and estimates of ancient CO₂ levels. *Global Biogeochemical Cycles* 6: 185–198.

Friedrich T, Timmermann A, Tigchelaar M, Timm EO, and Ganopolski A (2016) Nonlinear climate sensitivity and its implications for future greenhouse warming. *Science Advances* 2: e1501923. https://doi.org/10.1126/sciadv.1501923. pmid: 28861462.

Galvao Duarte A (2019) *Carbon and nitrogen dynamics in plants grown at low CO₂ conditions of the past.* Ph.D. Dissert., Univ. of West. Ontario, 174 pp.

Garrels RM and Lerman A (1984) Coupling of the sedimentary sulfur and carbon cycles; an improved model. *American Journal of Science* 284: 989–1007. https://doi.org/10.2475/ajs.284.9.989.

Garrels RM and Perry EA (1974) Cycling of carbon, sulfur, and oxygen through geologic time. In: Goldberg ED (ed.) *The Sea*, pp. 303–316. New York: Wiley.

Ghosh P and Bhattacharya SK (2001) CO₂ levels in the Late Palaeozoic and Mesozoic atmosphere from soil carbonate and organic matter, Satpura Basin, Central India. *Palaeogeography Palaeoclimatology Palaeoecology* 170: 219–236. https://doi.org/10.1016/S0031-0182(01)00237-1.

Ghosh P, Bhattacharya SK, and Ghosh P (2005) Atmospheric CO₂ during the late Paleozoic and Mesozoic: Estimates from Indian soils. In: Ehleringer JR, Cerling TE, and Dearing MD (eds.) *A History of Atmospheric CO₂ and Its Effects on Plants, Animals, and Ecosystems*, pp. 8–34. New York: Springer.

Goddéris Y and Donnadieu Y (2019) A sink- or a source-driven carbon cycle at the geological timescale? Relative importance of palaeogeography versus solid Earth degassing rate in the Phanerozoic climatic evolution. *Geological Magazine* 156: 355–365. https://doi.org/10.1017/S0016756817001054.

Goddéris Y, Donnadieu Y, Le Hir G, Lefebvre V, and Nardin E (2014) The role of palaeooceanography in the Phanerozoic history of atmopsheric CO₂ and climate. *Earth-Science Reviews* 128: 122–138.

Goddéris Y, Donnadieu Y, Lefebvre V, Le Hir G, and Nardin E (2012) Tectonic control of continental weathering, atmospheric CO₂, and climate over Phanerozoic times. *Comptes Rendus Geoscience* 344: 652–662. https://doi.org/10.1016/j.crte.2012.08.009.

Goddéris Y, Donnadieu Y, and Mills BJW (2023) What models tell us about the evolution of carbon sources and sinks over the Phanerozoic. *Annual Review of Earth and Planetary Sciences* 51: 471–492. https://doi.org/10.1146/annurev-earth-032320-092701.

Greenop R, Hain MP, Sosdian SM, Oliver KIC, Goodwin P, Chalk TB, Lear CH, Wilson PA, and Foster GL (2017) A record of Neogene seawater δ^{11}B reconstructed from paired δ^{11}B analyses on benthic and planktic foraminifera. *Climate of the Past* 13: 149–170.

Guitierrez K and Sheldon ND (2012) Paleoenvironmental reconstruction of Jurassic dinosaur habitats of the Vega Formation, Asturias, Spain. *Geological Society of America Bulletin* 124: 596–610. https://doi.org/10.1130/B30285.1.

Gulbranson EL, Tabor NJ, and Montañez IP (2011) A pedogenic geothithe record of soil CO₂ variations as a response to soil moisture content. *Geochimica et Cosmochimica Acta* 75(22): 7099–7116.

Gurung K, Field KJ, Batterman SA, Goddéris Y, Donnadieu Y, Porada P, Taylor LL, and Mills BJW (2022) Climate windows of opportunity for plant expansion during the Phanerozoic. *Nature Communications* 13: 4530. https://doi.org/10.1038/s41467-022-32077-7.

Hansen J, Sato M, Kharecha P, Beerling D, and Berner R (2008) Target atmospheric CO₂: Where should humanity aim? *The Open Atmospheric Science Journal* 2: 217–231. https://doi.org/10.2174/1874282300802010217.

Hansen J, Sato M, Simons L, Nazarenko LS, Sangha I, et al. (2023) Global warming in the pipeline. Open. *Climate Change* 3: kgad008. https://doi.org/10.1093/oxfclm/kgad008.

Haworth M, Hesselbo SP, McElwain JC, Robinson SA, and Brunt JW (2005) Mid Cretaceous pCO₂ based on stomata of the extinct conifer *Pseudofrenelopsis* (Cheirolepidiaceae). *Geology* 33: 749–752.

Haworth M, Heath J, and McElwain JC (2010) Differences in the response sensitivity of stomatal index to atmospheric CO₂ among four genera of Cupressaceae conifers. *Annals of Botany* 105: 411–418. https://doi.org/10.1093/aob/mcp309.

Henehan MJ, Rae JWB, Foster GL, Erez J, Prentice KC, Kucera M, Bostock HC, Martinez-Boti MA, Milton JA, Wilson PA, Marshall BJ, and Elliott T (2013) Calibration of the boron isotope proxy in the planktonic forminifera *Globigerinoides ruber* for use in palaeo-CO₂ reconstruction. *Earth and Planetary Science Letters* 364: 111–122. https://doi.org/10.1016/j.epsl.2012.12.029.

Henehan MJ, Foster GL, Bostock HC, Greenop R, Marshall BJ, and Wilson PA (2016) A new boron isotope-pH calibration for *Orbulina universa*, with implications for understanding and accounting for 'vital effects'. *Earth and Planetary Science Letters* 454: 282–292. https://doi.org/10.1016/j.epsl.2016.09.024.

Hesselbo SP, Robinson SA, Surlyk F, and Piasecki S (2002) Terrestrial and marine extinction at the Triassic–Jurassic boundary synchronized with major carbon-cycle perturbation: A link to initiation of massive volcanism? *Geology* 30: 251–254.

Higgins JA, Kurbatov AV, Spaulding NE, Brook E, Introne DS, Chimiak LM, Yan Y, Mayewski PA, and Bender ML (2015) Atmospheric composition 1 million years ago from blue ice in the Allan Hills, Antarctica. *Proceedings of the National Academy of Sciences of the United States of America* 112: 6887–6891. https://doi.org/10.1073/pnas.1420232112.

Hilton RG (2023) Earth's persistent thermostat. *Science* 379: 329–330.

Hilton RG and West AJ (2020) Mountains, erosion and the carbon cycle. *Nature Reviews Earth and Environment* 1: 284–299. https://doi.org/10.1038/s43017-020-0058-6.

Holland HD (1978) *The Chemistry of the Atmosphere and Oceans*. New York: Wiley.

Hollis CJ, Dunkley Jones T, Anagnostou E, et al. (2019) The DeepMIP contribution to PMIP4: Methodologies for selection, compilation and analysis of latest Paleocene and early Eocene climate proxy data, incorporating version 0.1 of the DeepMIP database. *Geoscientific Model Development* 12: 3149–3206. https://doi.org/10.5194/gmd-12-3149-2019.

Hong SK and Lee YI (2012) Evaluation of atmospheric carbon dioxide concentrations during the Cretaceous. *Earth and Planetary Science Letters* 327–328: 23–28. https://doi.org/10.1016/j.epsl.2012.01.014.

Hönisch B and Hemming NG (2005) Surface ocean pH response to variations in pCO₂ through two full glacial cycles. *Earth and Planetary Science Letters* 236: 305–314.

Hönisch B, Eggins SM, Haynes LL, Allen KA, Holland KD, and Lorbacher K (2019) *Boron Proxies in Paleoceanography and Paleoclimatology*, p. 256. Wiley-Blackwell.

Hönisch B, Fish CR, Phelps SR, Haynes LL, Dyez K, Holland K, Fehrenbacher J, Allen KA, Eggins S, and Goes JI (2021) Symbiont photosynthesis and its effect on Boron proxies in planktic foraminifera. *Paleoceanography and Paleoclimatology* 36. https://doi.org/10.1029/2020PA004022. e2020PA004022.

Hope C (2015) The $10 trillion value of better information about the transient climate response. *Philosophical Transactions. Series A, Mathematical, Physical, and Engineering Sciences* 373: 20140429. https://doi.org/10.1098/rsta.2014.0429.

Hsieh JCC and Yapp CJ (1999) Stable carbon isotope budget of CO₂ in a wet, modern soil as inferred from Fe(CO3)OH in pedogenic goethite: Possible role of calcite dissolution. *Geochimica et Cosmochimica Acta* 63: 767–783.

Huang CM, Retallack GJ, and Wang CS (2012) Early Cretaceous atmospheric pCO₂ levels recorded from pedogenic carbonates in China. *Cretaceous Research* 33: 42–49. https://doi.org/10.1016/j.cretres.2011.08.001.

Huber M and Caballero R (2011) The early Eocene equable climate problem revisited. *Climate of the Past* 7: 603–633. https://doi.org/10.5194/cp-7-603-2011.

Huber BT, MacLeod KG, Watkins DK, and Coffin MF (2018) The rise and fall of the Cretaceous Hot Greenhouse climate. *Global and Planetary Change* 167: 1–23. https://doi.org/10.1016/j.gloplacha.2018.04.004.

Hull PM, Bornemann A, Penman DE, Henehan MJ, Norris RD, et al. (2020) On impact and volcanism across the Cretaceous-Paleogene boundary. *Science* 367: 266–272. https://doi.org/10.1126/science.aay5055.

Hutchinson DK, Coxall HC, Lunt DJ, Steinthorsdottir M, de Boer AM, et al. (2021) The Eocene–Oligocene transition: A review of marine and terrestrial proxy data, models and model-data comparisons. *Climate of the Past* 17: 269–315. https://doi.org/10.5194/cp-17-269-2021.

Ibarra DE, Rugenstein JKC, Bachan A, Baresch A, Lau KV, Thomas DL, Lee J-E, Boyce CK, and Chamberlain CP (2019) Modeling the consequences of land plant evolution on silicate weathering. *American Journal of Science* 319: 1–43. https://doi.org/10.2475/01.2019.01.

IPCC (2021) Summary for policymakers. In: Masson-Delmotte V, Zhai P, Pirani A, Connors SL, Pean C, et al. (eds.) *Climate Change 2021: The Physical Science Basis Contribution of Working Group I to the Sixth Assessment Report of the Intergovernmental Panel on Climate*, pp. 3–32. Cambridge, United Kingdom and New York, NY, USA: Change Cambridge University Press. https://doi.org/10.1017/9781009157896.001.

IPCC (2022) Summary for policymakers. In: Pörtner H-O, Roberts DC, Poloczanska DC, Mintenbeck K, Tignor M, et al. (eds.) *Climate Change 2022: Impacts, Adaptation and Vulnerability. Contribution of Working Group II to the Sixth Assessment Report of the Intergovernmental Panel on Climate Change*, pp. 3–33. Cambridge, UK and New York, NY, USA: Cambridge University Press. https://doi.org/10.1017/9781009325844.001.

Isson TT and Planavsky NJ (2018) Reverse weathering as a long-term stabilizer of marine pH and planetary climate. *Nature* 560: 471–475.

Isson TT, Zhang S, Lau KV, Rauzi S, Tosca NJ, Penman DE, and Planavsky NJ (2022) Marine siliceous ecosystem decline led to sustained anomalous Early Triassic warmth. *Nature Communications* 13: 3509. https://doi.org/10.1038/s41467-022-31128-3.

Jacob R (1997) *Low frequency variability in a simulated atmosphere ocean system*. Ph.D. dissertation,. Univ. Wisc.-Madison. 155 pp.

Jagniecki EA, Lowenstein TK, Jenkins DM, and Demicco RV (2015) Eocene atmospheric CO$_2$ from the nahcolite proxy. *Geology* 43: 1075–1078.

Jenkyns HC (2010) Geochemistry of oceanic anoxic events. *Geochemistry, Geophysics, Geosystems* 11. https://doi.org/10.1029/2009GC002788. Q03004.

Jing D and Banian S (2018) Early Cretaceous atmospheric CO$_2$ estimates based on stomatal index of *Pseudofrenelopsis papillosa* (Cheirolepidiaceae) from southeast China. *Cretaceous Research* 85: 232–242. https://doi.org/10.1016/j.cretres.2017.08.011.

Kasting JF (1989) Long-Term Stability of the Earth's climate. *Palaeogeography Palaeoclimatology Palaeoecology* 75: 83–95.

Keller G (2014) Deccan volcanism, the Chicxulub impact, and the end-Cretaceous mass extinction: Coincidence? Cause and effect? In: Keller G and Kerr AC (eds.) *Volcanism, Impacts, and Mass Extinctions: Causes and Effects*, pp. 57–89. https://doi.org/10.1130/2014.2505(03). Geol. Soc. Amer. Spec. Publ. 505.

Kohn MJ (2016) Carbon isotope discrimination in C3 land plants is independent of natural variations in p$_{CO2}$. *Geochemical Perspectives Letters* 2: 35–43.

Konrad W, Roth-Nebelsick A, and Grein M (2008) Modelling of stomatal density response to atmospheric CO$_2$. *Journal of Theoretical Biology* 253: 638–658.

Kowalczyk JB, Royer DL, Miller IM, Anderson CW, Beerling DJ, Franks PJ, Grein M, Konrad W, Roth-Nebelsick A, Bowring SA, Johnson KR, and Ramezani J (2018) Multiple Proxy Estimates of Atmospheric CO$_2$ From an Early Paleocene Rainforest. *Paleoceanography and Paleoclimatology* 33: 1427–1438. https://doi.org/10.1029/2018PA003356.

Krause AJ, Mills BJW, Zhang S, Planavsky NJ, Lenton TM, and Poulton SW (2018) Stepwise oxygenation of the Paleozoic atmosphere. *Nature Communications* 9: 4081. https://doi.org/10.1038/s41467-018-06383-y.

Krissansen-Totton J and Catling DC (2017) Constraining climate sensitivity and continental versus seafloor weathering using an inverse geological carbon cycle model. *Nature Communications* 8: 15423. https://doi.org/10.1038/ncomms15423.

Kürschner WM, Kvacek Z, and Dilcher DL (2008) The impact of Miocene atmospheric carbon dioxide fluctuations on climate and the evolution of terrestrial ecosystems. *Proceedings of the National Academy of Sciences* 105: 449–453. https://doi.org/10.1073/pnas.0708588105.

Lee Y Il (1999) Stable isotopic composition of calcic paleosols of the Early Cretaceous Hasandong Formation, southeastern Korea. *Palaeogeography Palaeoclimatology Palaeoecology* 150: 123–133.

Lee Y Il and Hisada K (1999) Stable isotopic composition of pedogenic carbonates of the Early Cretaceous Shimonoseki Subgroup, western Honshu, Japan. *Palaeogeography, Palaeoclimatology, Palaeoecology* 153: 127–138.

Lee C-TA, Shen B, Slotnick BS, Liao K, Dickens GR, Yokoyama Y, Lenardic A, Dasgupta R, Jellinek M, Lackey JS, Schneider T, and Tice MM (2013) Continental arc–island arc fluctuations, growth of crustal carbonates, and long-term climate change. *Geosphere* 9: 21–36. https://doi.org/10.1130/ges00822.1.

Lee J-Y, et al. (2021) Future global climate: Scenario-based projections and near-term information. In: Masson-Delmotte V, Zhai P, Pirani A, Connors SL, Pean C, et al. (eds.) *Climate Change 2021: The Physical Science Basis Contribution of Working Group I to the Sixth Assessment Report of the Intergovernmental Panel on Climate*, pp. 553–672. Cambridge, United Kingdom and New York, NY, USA: Change Cambridge University Press. https://doi.org/10.1017/9781009157896.006.

Leier A, Quade J, DeCelles P, and Kapp P (2009) Stable isotopic results from paleosol carbonate in South Asia: Paleoenvironmental reconstructions and selective alteration. *Earth and Planetary Science Letters* 279: 242–254. https://doi.org/10.1016/j.epsl.2008.12.044.

Lemarchand D, Gaillardet J, Lewin É, and Allègre CJ (2000) The influence of rivers on marine boron isotopes and implications for reconstructing past ocean pH. *Nature* 408: 951–954. https://doi.org/10.1038/35050058.

Lenton TM, Crouch M, Johnson M, Pires N, and Dolan L (2012) First plants cooled the Ordovician. *Nature Geoscience* 5: 86–89. https://doi.org/10.1038/ngeo1390.

Lenton TM, Dahl TW, Daines SJ, Mills BJW, Ozaki K, Saltzman MR, and Porada P (2016) Earliest land plants created modern levels of atmospheric oxygen. *Proceedings of the National Academy of Sciences* 113: 9704–9709. www.pnas.org/cgi/doi/10.1073/pnas.1604787113.

Lenton TM, Daines SJ, and Mills BJW (2018) COPSE reloaded: An improved model of biogeochemical cycling over Phanerozoic time. *Earth Science Reviews* 178: 1–28. https://doi.org/10.1016/j.earscirev.2017.12.004.

Li X, Jenkyns HC, Zhang C, Wang Y, Liu L, and Cao K (2014) Carbon isotope signatures of pedogenic carbonates from SE China: Rapid atmospheric pCO2 changes during middle–late Early Cretaceous time. *Geological Magazine* 151: 830–849. https://doi.org/10.1017/S0016756813000897.

Li J, Wen XY, and Huang CM (2016) Lower Cretaceous paleosols and paleoclimate in Sichuan Basin, China. *Cretaceous Research* 62: 154–171. https://doi.org/10.1016/j.cretres.2015.10.002.

Li H, Yu J, McElwain JC, Yiotis C, and Chen Z-Q (2019) Reconstruction of atmospheric CO$_2$ concentration during the late Changhsingian based on fossil conifers from the Dalong Formation in South China. *Palaeogeography Palaeoclimatology Palaeoecology* 519: 37–48. https://doi.org/10.1016/j.palaeo.2018.09.006.

Li X, Wang J, Rasbury T, Zhou M, Wei Z, and Zhang C (2020) Early Jurassic climate and atmospheric CO$_2$ concentration in the Sichuan paleobasin, southwestern China. *Climate of the Past* 16: 2055–2074. https://doi.org/10.5194/cp-16-2055-2020.

Lomax BH, Lake JA, Leng MJ, and Jardine PE (2019) An experimental evaluation of the use of Δ^{13}C as a proxy for palaeoatmospheric CO$_2$. *Geochimica et Cosmochimica Acta* 247: 162–174.

Longman J, Mills BJW, Mannes HR, Gernon TM, and Palmer MR (2021) Late Ordovician climate change and extinctions driven by elevated volcanic nutrient supply. *Nature Geoscience* 14: 924–929.

Looy CV, Twitchett RJ, Dilcher DL, van Konijnenburg-van Cittert JHA, and Visscher H (2001) Life in the end-Permian dead zone. *Proceedings of the National Academy of Sciences* 98: 7879–7883. www.pnas.orgycgiydoiy10.1073ypnas.131218098.

Lowenstein TK and Demicco RV (2006) Elevated Eocene atmospheric CO$_2$ and its subsequent decline. *Science* 313: 1928.

Lucas SG and Tanner LH (2021) Late Pennsylvanian calcareous paleosols from central New Mexico: Implications for paleoclimate. *New Mexico Geology* 43: 3–9. https://doi.org/10.58799/NMG-v43n1.3.

Ludvigson GA, Joeckel RM, Murphy LR, Stockli DF, González LA, Suarez CA, Kirkland JI, and Al-Suwaidi A (2015) The emerging terrestrial record of Aptian-Albian global change. *Cretaceous Research* 56: 1–24. https://doi.org/10.1016/j.cretres.2014.11.008.

Lunt DJ, Haywood AM, Schmidt GA, Salzmann U, Valdes PJ, and Dowsett HJ (2010) Earth system sensitivity inferred from Pliocene modelling and data. *Nature Geoscience* 3: 60–64. https://doi.org/10.1038/NGEO706.

Macarewich SI, Poulsen CJ, and Montañez IP (2021) Simulation of oxygen isotopes and circulation in a late Carboniferous epicontinental seas with implications for proxy records. *Earth and Planetary Science Letters* 559: 116770. https://doi.org/10.1016/j.epsl.2021.116770.

Macdonald FA, Swanson-Hysell NL, Park Y, Lisiecki L, and Jagoutz O (2019) Arc-continent collisions in the tropics set Earth's climate state. *Science* 364: 181–184. https://doi.org/10.1126/science.aav5300.

Maffre P, Swanson-Hysell NL, and Goddéris Y (2021) Limited Carbon Cycle Response to Increased Sulfide Weathering Due to Oxygen Feedback. *Geophysical Research Letters* 48. e2021GL094589.

Marcilly CM, Torsvik TH, Domeier M, and Royer DL (2021) New paleogeographic and degassing parameters for long-term carbon cycle models. *Gondwana Research* 97: 176–203. https://doi.org/10.1016/j.gr.2021.05.016.

Marzoli AS, Callegaro J, Dal Corso JH, Davies M, Chiaradia N, Youbi H, Bertrand L, Reisberg R, and Merle FJ (2018) The Central Atlantic magmatic province (CAMP): A review. In: Tanner LH (ed.) *The Late Triassic World*, pp. 91–125. Syracuse, New York: Springer.

Matthaeus WJ, Macarewich S, Richey JD, Wilson JP, McElwain JC, Montañez IP, DiMichele WA, Hren MT, Poulsen CJ, and White JD (2021) Evolution of freeze tolerance influenced plant distributions and hydrology during the penultimate ice age. *Proceedings of the National Academy of Sciences of the United States of America* 118(42). https://doi.org/10.1073/pnas.2025227118.

Matthaeus WJ, Macarewich SI, Richey J, Montañez IP, McElwain JC, White JD, Wilson JP, and Poulsen CJ (2023) A systems approach to understanding how plants transformed Earth's environment in deep time. *Annual Reviews in Earth and Planetary Sciences* 51: 551–580. https://doi.org/10.1146/annurev-earth-080222-082017.

Mays C, Steinthorsdottir M, and Stilwell JD (2015) Climatic implications of *Ginkgoites waarrensis* Douglas emend. from the south polar Tupuangi flora, Late Cretaceous (Cenomanian), Chatham Islands. *Palaeogeography Palaeoclimatology Palaeoecology* 438: 308–326.

McElwain JC (1998) Do fossil plants signal palaeoatmospheric CO₂ concentration in the geological past? *Philosophical Transactions of the Royal Society of London B* 353: 83–96.

McElwain JC and Punyasena SW (2007) Mass extinction events and the plant fossil record. *Trends in Ecology & Evolution* 22: 548–557.

McElwain JC and Steinthorsdottir M (2017) Palaeoecology, ploidy, palaeoatmospheres and developmental biology: A review of fossil stomata. *Plant Physiology* 174. https://doi.org/10.1104/pp.17.00204. 00204.2017.

McElwain JC, Beerling D, and Woodward FI (1999) Fossil plants and global warming at the Triassic–Jurassic boundary. *Science* 285: 1386–1390.

McElwain JC, Wade-Murphy J, and Hesselbo SP (2005) Changes in carbon dioxide during an oceanic anoxic event linked to intrusion into Gondwana coals. *Nature* 435: 479–482.

McKenzie NR and Jiang H (2019) Earth's outgassing and climatic transitions: The slow burn toward environmental "catastrophes"? *Elements* 15: 325–330. https://doi.org/10.2138/gselements.15.5.325.

McKenzie NR, Horton BK, Loomis SE, Stockli DF, Planavsky NJ, and Lee C-TA (2016) Continental arc volcanism as the principal driver of icehouse-greenhouse variability. *Science* 352: 444–447. https://doi.org/10.1126/science.aad5787.

Mcloughlin S (2012) Glossopteris - insights into the architecture and relationships of an iconic Permian Gondwanan plant. *Journal of the Botanical Society of Bengal* 65: 1–14.

Milligan JN, Royer DL, Franks PJ, Upchurch GR, and McKee ML (2019) No evidence for a Large Atmospheric CO₂ Spike across the Cretaceous-Paleogene Boundary. *Geophysical Research Letters* 46: 3462–3472. https://doi.org/10.1029/2018GL081215.

Mills BJW, Krause AJ, Scotese CR, Hill DJ, Shields GA, and Lenton TM (2019) Modelling the long-term carbon cycle, atmospheric CO₂, and Earth surface temperature from late Neoproterozoic to present day. *Gondwana Research* 67: 172–186. https://doi.org/10.1016/j.gr.2018.12.001.

Mills B, Daines SJ, and Lenton TM (2014) Changing tectonic controls on the long-term carbon cycle from Mesozoic to present. *Geochemistry, Geophysics, Geosystems* 15(12): 4866–4884.

Mills BJW, Donnadieu Y, and Goddéris Y (2021) Spatial continuous integration of Phanerozoic global biogeochemistry and climate. *Gondwana Research* 100: 73–86. https://doi.org/10.1016/j.gr.2021.02.011.

Mills BJW, Krause AJ, Jarvis I, and Cramer BD (2023) Evolution of atmospheric O₂ through the Phanerozoic, revisited. *Annual Review of Earth and Planetary Sciences* 51: 253–276. https://doi.org/10.1146/annurev-earth-032320-095425.

Montañez IP (2013) Modern soil system constraints on reconstructing deep-time atmospheric CO₂. *Geochimica et Cosmochimica Acta* 101: 57–75.

Montañez IP (2022) Current synthesis of the penultimate icehouse and its imprint on the Upper Devonian through Permian stratigraphic record. In: Lucas S, Schneider JW, Wang X, and Nikolaeva S (eds.) *The Carboniferous Timescale*, pp. 213–245. https://doi.org/10.1144/SP512-2021-124. Geol. Soc., London, Spec. Publ. 512, London.

Gulbranson EL, Montañez IP, and Tabor NJ (2011) Determining ancient humidity and floral provinces from paleosols: A climate proxy derived from a pedogenic energy model and modern soil geochemistry. *Journal of Geology* 119: 559–573.

Montañez IP, Tabor NJ, Niemeier D, DiMichele WA, Frank TD, Fielding CR, Isbell JL, Birgenheier LP, and Rygel MC (2007) CO₂-Forced Climate and Vegetation Instability during Late Paleozoic Deglaciation. *Science* 315: 87–91. https://doi.org/10.1126/science.11342.

Montañez IP, McElwain JC, Poulsen CJ, White JD, DiMichele WA, Wilson JP, Griggs G, and Hren MT (2016) Climate, pCO₂ and terrestrial carbon cycle linkages during late Palaeozoic glacial-interglacial cycles. *Nature Geoscience* 9: 824–828. https://doi.org/10.1038/ngeo2822.

Mora CI, Driese SG, and Colarusso LA (1996) Middle and late Paleozoic atmospheric CO₂ levels from soil carbonate and organic matter. *Science* 271: 1105–1107. https://doi.org/10.1126/science.271.5252.1105.

Morgan JV, Bralower TJ, Brugger J, and Wünnemann K (2022) The Chicxulub impact and its environmental consequences. *Nature Reviews Earth and Environment* 3: 338–354. https://doi.org/10.1038/s43017-022-00283-y.

Mortazavi M, Moussavi-Harami R, Brenner RL, Mahboubi A, and Nadjafi M (2013) Stable isotope record in pedogenic carbonates in northeast Iran: Implications for Early Cretaceous (Berriasian–Barremian) paleovegetation and paleoatmospheric P(CO₂) levels. *Geoderma* 211–212: 85–97. https://doi.org/10.1016/j.geoderma.2013.07.008.

Müller RD, Mather B, Dutkiewicz A, Keller T, Merdith A, Gonzalez CM, Gorczyk W, and Zahirovic S (2022) Evolution of Earth's tectonic carbon conveyor belt. *Nature* 605: 629–639. https://doi.org/10.1038/s41586-022-04420-x.

Nordt L, Atchley S, and Dworkin S (2002) Paleosol barometer indicates extreme fluctuations in atmospheric CO₂ across the Cretaceous-Tertiary boundary. *Geology* 30: 703–706. https://doi.org/10.1130/0091-7613(2002)030<0703:PBIEFI>2.0.CO;2.

Nordt LC, Atchley S, and Dworkin S (2003) Terrestrial evidence for two greenhouse events in the latest Cretaceous. *GSA Today* 13(12): 4–9.

Nordt LC, Atchley S, and Dworkin S (2015) Collapse of the Late Triassic megamonsoon in western equatorial Pangea, present-day American Southwest. *Bulletin Geological Society of America* 127: 1798–1815. https://doi.org/10.1130/b31186.1.

Pagani M, Freeman KH, Ohkouchi N, and Caldeira K (2002) Comparison of water column [CO2aq] with sedimentary alkenone-based estimates: A test of the alkenone CO₂-proxy. *Paleoceanography* 17. https://doi.org/10.1029/2002PA000756.

Pagani M, Zachos JC, Freeman KH, Tipple B, and Bohaty S (2005) Marked Decline in Atmospheric Carbon Dioxide Concentrations During the Paleogene. *Science* 309: 600–603.

Palazzo Corner S, Siegert M, Ceppi P, Fox-Kemper B, Frolicher TL, et al. (2023) The zero emissions commitment and climate stabilization. *Frontiers in Science* 1: 1170744. https://doi.org/10.3389/fsci.2023.1170744.

Pall J, Zahirovic S, Doss S, Hassan R, Matthews KJ, Cannon J, Gurnis M, Moresi L, Lenardic A, and Müller RD (2018) The influence of carbonate platform interactions with subduction zone volcanism on palaeo-atmospheric CO₂ since the Devonian. *Climate of the Past* 14: 857–870. https://doi.org/10.5194/cp-14-857-2018.

Park J and Royer DL (2011) Geologic constraints on the glacial amplification of Phanerozoic climate sensitivity. *American Journal of Science* 311: 1–26. https://doi.org/10.2475/01.2011.01.

Passalia MG (2009) Cretaceous pCO₂ estimation from stomatal frequency analysis of gymnosperm leaves of Patagonia, Argentina. *Palaeogeography, Palaeoclimatology, Palaeoecology* 272: 17–24. https://doi.org/10.1016/j.palaeo.2008.11.010.

Phelps SR, Hennon GMM, Dyhrman ST, Hernandez Limon MD, Williamson OM, and Polissar PJ (2021) Carbon Isotope Fractionation in Noelaerhabdaceae Algae in Culture and a Critical Evaluation of the Alkenone Paleobarometer. *Geochemistry, Geophysics, Geosystems* 22. https://doi.org/10.1029/2021GC009657. e2021GC009657.

Pienkowski G, Hesselbo SP, Barbacka M, and Leng MJ (2020) Non-marine carbon-isotope stratigraphy of the Triassic-Jurassic transition in the Polish Basin and its relationships to organic carbon preservation, pCO₂ and palaeotemperature. *Earth Science Reviews* 210: 103383. https://doi.org/10.1016/j.earscirev.2020.103383.

Porter AS, Yiotis C, Montañez IP, and McElwain JC (2017) Evolutionary differences in Δ¹³C detected between spore and seed bearing plants following exposure to a range of atmospheric O₂:CO₂ ratios; implications for paleoatmosphere reconstruction. *Geochimica et Cosmochimica Acta* 213: 517–533.

Porter AS, Evans-Fitz, Gerald C, Yiotis C, Montañez IP, and McElwain JC (2019) Testing the accuracy of new paleoatmospheric CO₂ proxies based on plant stable carbon isotopic composition and stomatal traits in a range of simulated paleoatmospheric O₂:CO₂ ratios. *Geochimica et Cosmochimica Acta* 259: 69–90.

Price GD, Főzy I, and Pálfy J (2016) Carbon cycle history through the Jurassic–Cretaceous boundary: A new global δ13C stack. *Palaeogeography Palaeoclimatology Palaeoecology* 451: 46–61. https://doi.org/10.1016/j.palaeo.2016.03.016.

Prochnow SJ, Nordt LC, Atchley SC, and Hudec MR (2006) Multi-proxy paleosol evidence for middle and late Triassic climate trends in eastern Utah. *Palaeogeography Palaeoclimatology Palaeoecology* 232: 53–72. https://doi.org/10.1016/j.palaeo.2005.08.011.

Qiu Z, Zou C, Mills BJW, Xiong Y, Tao H, Lu B, Liu H, Xiao W, and Pouton SW (2022) A nutrient control on expanded anoxia and global cooling during the Late Ordovician mass extinction. *Communications Earth & Environment* 3: 1–9. https://doi.org/10.1038/s43247-022-00412-x.

Quan C, Sun C, Sun Y, and Sun G (2009) High resolution estimates of paleo-CO$_2$ levels through the Campanian (Late Cretaceous) based on *Ginkgo* cuticles. *Cretaceous Research* 30: 424–428.

Quirk J, Leake JR, Johnson DA, Taylor LL, Saccone L, and Beerling DJ (2015) Constraining the role of early land plants in Palaeozoic weathering and global cooling. *Proceedings of the Biological Sciences* 282: 20151115.

Rae JWB (2018) Boron Isotopes in Foraminifera: Systematics, Biomineralisation, and CO$_2$ Reconstruction. In: Marschall H and Foster G (eds.) *Boron Isotopes. Advances in Isotope Geochemistry*. Springer. https://doi.org/10.1007/978-3-319-64666-4_5. Cham.

Raitzsch M and Hönisch B (2013) Cenozoic boron isotope variations in benthic foraminifers. *Geology* 41: 591–594.

Rau GH, Riebesell U, and Wolf-Gladrow D (1996) A model of photosynthetic 13C fractionation by marine phytoplankton based on diffusive molecular CO$_2$ uptake. *Marine Ecology Progress Series* 133: 275–285.

Renne PR, Sprain CJ, Richards MA, Self S, Vanderkluysen L, and Pande K (2015) State shift in Deccan volcanism at the Cretaceous-Paleogene boundary, possibly induced by impact. *Science* 350: 76–78.

Retallack GJ (2009) Greenhouse crises of the past 300 million years. *Geological Society of America Bulletin* 121: 1441–1455.

Richey JD, Upchurch GR, Montañez IP, Lomax BH, Suarez MB, Crout NMJ, Joeckel RM, Ludvigson GA, and Smith JJ (2018) Changes in CO$_2$ during Oceanic Anoxic Event 1d indicate similarities to other carbon cycle perturbations. *Earth and Planetary Science Letters* 491: 172–182. https://doi.org/10.1016/j.epsl.2018.03.035.

Richey JD, Montañez IP, Goddéris Y, Looy CV, Griffis NP, and DiMichele WA (2020) Influence of temporally varying weatherability on CO$_2$—climate coupling and ecosystem change in the late Paleozoic. *Climate of the Past* 16: 1759–2020. https://doi.org/10.5194/cp-16-1759-2020.

Robinson SA, Andrews JE, Hesselbo SP, Radley JD, Dennis PF, Harding IC, and Allen P (2002) Atmospheric pCO$_2$ and depositional environment from stable-isotope geochemistry of calcrete nodules (Barremian, Lower Cretaceous, Wealden Beds, England). *Journal of the Geological Society of London* 159: 215–224. https://doi.org/10.1144/0016-764901-015.

Rohling E, Sluijs A, Dijkstra H, Köhler P, van de Wal R, et al. (2012) Making sense of palaeoclimate sensitivity. *Nature* 491: 683–691. https://doi.org/10.1038/nature11574.

Rost B, Zondervan I, and Riebesell U (2002) Light-dependent carbon isotope fractionation in the coccolithophorid Emiliania huxleyi. *Limnology and Oceanography* 47: 120–128.

Roth-Nebelsick A and Konrad W (2003) Assimilation and transpiration capabilities of rhyniophytic plants from the Lower Devonian and their implications for palaeoatmospheric CO$_2$ concentration. *Palaeogeography Palaeoclimatology Palaeoecology* 202: 153–178. https://doi.org/10.1016/S0031-0182(03)00634-5.

Royer DL (2014) Atmospheric CO$_2$ and O$_2$ during the Phanerozoic: Tools, patterns, and impacts. In: Holland HD and Turekian KK (eds.) *Treatise on Geochemistry*, Second Edition, pp. 251–267. Oxford: Elsevier. https://doi.org/10.1016/B978-0-08-095975-7.01311-5.

Royer DL (2016) Climate sensitivity in the geologic past. *Annual Review of Planetary Science* 44: 277–293. https://doi.org/10.1146/annurev-earth-100815-024150.

Royer DL, Berner RA, and Beerling DJ (2001) Phanerozoic atmospheric CO$_2$ change: Evaluating geochemical and paleobiological approaches. *Earth Science Reviews* 54: 349–392.

Royer DL, Berner RA, Montañez IP, Tabor NJ, and Beerling DJ (2004) CO$_2$ as a primary driver of Phanerozoic climate. *GSA Today* 14: 4–10.

Royer DL, Berner RA, and Park J (2007) Climate sensitivity constrained by CO$_2$ concentrations over the past 420 million years. *Nature* 446: 530–532. https://doi.org/10.1038/nature05699.

Royer DL, Donnadieu Y, Park J, Kowalczyk J, and Goddéris Y (2014) Error analysis of CO$_2$ and O$_2$ estimates from the long-term geochemical model GEOCARBSULF. *American Journal of Science* 314: 1259–1283. https://doi.org/10.2475/09.2014.01.

Schaller MF, Wright JD, and Kent DV (2011) Atmospheric pCO$_2$ perturbations associated with the Central Atlantic Magmatic Province. *Science* 331: 1404–1409.

Schaller MF, Wright JD, and Kent DV (2015) A 30 Myr record of Late Triassic atmospheric pCO$_2$ variation reflects a fundamental control of the carbon cycle by changes in continental weathering. *Bulletin Geological Society of America* 127: 661–671. https://doi.org/10.1130/b31107.1.

Scher MA, Barclay RS, Baczynski AA, Smith BA, and Sappington J (2022) The effect of CO$_2$ concentration on carbon isotope discrimination during photosynthesis in *Ginkgo biloba*: Implications for reconstructing atmospheric CO$_2$ levels in the geologic past. *Geochimica et Cosmochimica Acta* 337: 82–94. https://doi.org/10.1016/j.gca.2022.09.033.

Schlanser K, Diefendorf AF, Greenwood DR, Mueller KE, West CK, Lowe AL, and Basinger JD (2020) On geologic timescales, plant carbon isotope fractionation responds to precipitation similarly to modern plants and has a small negative correlation with pCO$_2$. *Geochimica et Cosmochimica Acta* 270: 264–281.

Schroeder PA and Melear ND (1999) Stable carbon isotope signatures preserved in authigenic gibbsite from a forested granitic-regolith: Panola Mt., Georgia, USA. *Geoderma* 91: 261–279.

Schubert BA and Jahren AH (2012) The effect of atmospheric CO$_2$ concentration on carbon isotope fractionation in C3 land plants. *Geochimica et Cosmochimica Acta* 96: 29–43.

Schubert BA and Jahren AH (2015) Global increase in plant carbon isotope fractionation following the Last Glacial Maximum caused by increase in atmospheric pCO$_2$. *Geology* 43: 435–438.

Schubert BA and Jahren AH (2018) Incorporating the effects of photorespiration into terrestrial paleoclimate reconstruction. *Earth-Science Reviews* 177: 637–642. https://doi.org/10.1016/j.earscirev.2017.12.00.

Schulte P, Alegret L, Arenillas I, Arz JA, Barton PJ, et al. (2010) The Chicxulub asteroid impact and mass extinction at the Cretaceous–Paleogene boundary. *Science* 327: 1214–1218.

Sherwood SC, Webb MJ, Annan JD, Armour KC, Forster PM, et al. (2020) An assessment of Earth's climate sensitivity using multiple lines of evidence. *Reviews of Geophysics* 58. https://doi.org/10.1029/2019RG000678. e2019RG000678.

Shields GA and Mills BJW (2021) Evaporite weathering and deposition as a long-term climate forcing mechanism. *Geology* 49: 299–303.

Slodownik M, Vajda V, and Steinthorsdottir M (2021) Fossil seed fern *Lepidopteris ottonis* from Sweden records increasing CO$_2$ concentration during the end-Triassic extinction event. *Palaeogeography Palaeoclimatology Palaeoecology* 564. https://doi.org/10.1016/j.palaeo.2020.110157.

Somelar P, Soomera S, Driese SG, Lepland A, Stinchcomb GE, and Kirsimäe K (2020) CO$_2$ drawdown and cooling at the onset of the Great Oxidation Event recorded in 2.45 Ga paleoweathering crust. *Chemical Geology* 548: 119678. https://doi.org/10.1016/j.chemgeo.2020.119678.

Stanley SM (2016) Estimates of the magnitudes of major marine mass extinctions in Earth history. *Proceedings of the National Academy of Sciences* 113(42): E6325–E6334. https://doi.org/10.1073/pnas.1613094113.

Steinthorsdottir M and Vajda V (2015) Early Jurassic (late Pliensbachian) CO$_2$ concentrations based on stomatal analysis of fossil conifer leaves from eastern Australia. *Gondwana Research* 27: 932–939.

Steinthorsdottir M, Jeram AJ, and McElwain JC (2011) Extremely elevated CO$_2$ concentrations at the Triassic/Jurassic Boundary. *Palaeogeography Palaeoclimatology Palaeoecology* 308: 418–432.

Steinthorsdottir M, Porter AS, Holohan A, Kunzmann L, Collinson M, and McElwain JC (2016a) Fossil plant stomata indicate decreasing atmospheric CO$_2$ prior to the Eocene–Oligocene boundary. *Climate of the Past* 11: 4985–5019.

Steinthorsdottir M, Vajda V, and Pole M (2016b) Global trends of pCO$_2$ across the Cretaceous-Paleogene boundary supported by the first Southern Hemisphere stomatal proxy-based pCO$_2$ reconstruction. *Palaeogeography Palaeoclimatology Palaeoecology*: 143–152.

Steinthorsdottir M, Elliott-Kingston C, and Bacon KL (2018) Cuticle surfaces of fossil plants as a potential proxy for volcanic SO$_2$ emissions: Observations from the Triassic-Jurassic transition of East Greenland. *Palaeobiodiversity and Palaeoenvironments* 98: 49–69.

Steinthorsdottir M, Vajda V, Pole M, and Holdgate G (2019a) Moderate levels of Eocene pCO$_2$ indicated by fossil plant stomata. *Geology* 47: 914–918.

Steinthorsdottir M, Vajda V, and Pole M (2019b) Significant transient pCO₂ perturbation across the New Zealand Oligocene-Miocene transition recorded by fossil plants. *Palaeogeography Palaeoclimatology Palaeoecology* 515: 152–161.

Steinthorsdottir M, Jardine PE, and Rember WC (2021) Near-Future pCO₂ During the Hot Miocene Climatic Optimum. *Palaeogeography Palaeoclimatology Palaeoecology* 36. e2020PA003900.

Steinthorsdottir M, Jardine PE, Lomax BH, and Sallstedt T (2022) Key traits of living fossil *Ginkgo biloba* are highly variable but not influenced by climate – Implications for palaeo-pCO₂ reconstructions and climate sensitivity. *Global and Planetary Change* 211. https://doi.org/10.1016/j.gloplacha.2022.103786. 103786.

Stoll HM, Guitian J, Hernandez-Almeida I, Mejia LM, Phelps S, Polissar P, Rosenthal Y, Zhang H, and Ziveri P (2019) Upregulation of phytoplankton carbon concentrating mechanisms during low CO₂ glacial periods and implications for the phytoplankton pCO₂ proxy. *Quaternary Science Reviews* 208: 1–20.

Suarez MB, Knight JA, Godet A, Ludvigson GA, Snell KE, Murphy L, and Kirkland JL (2021) Multiproxy strategy for determining palaeoclimate parameters in the Ruby Ranch Member of the Cedar Mountain Formation. In: Bojar AV, Pelc A, and Lecuyer C (eds.) *Stable Isotope Studies of the Water Cycle and Terrestrial Environments*, pp. 313–334. https://doi.org/10.1144/SP507-2020-85. Geol. Soc. London, Special Pub. 507.

Sun B, Xiao L, Xie S, Deng S, Wang Y, Jia H, and Turner S (2007) Quantitative analysis of paleoatmospheric CO₂ level based on stomatal characters of fossil *Ginkgo* from Jurassic to Cretaceous of China. *Acta Geologica Sinica* 81: 931–939.

Tabor NJ and Yapp CJ (2005) Incremental vacuum dehydration-decarbonation experiments on a natural gibbsite (α-AI (OH3)): CO₂ abundance and δ^{13}C values. *Geochimica et Cosmochimica Acta* 69: 519–527.

Tabor NJ, Yapp CJ, and Montañez IP (2004) Goethite, calcite, and organic matter from Permian and Triassic soils: Carbon isotopes and atmospheric CO₂ concentrations. *Geochimica et Cosmochimica Acta* 68: 1503–1517.

Tanner LH, Hubert JF, Coffey BP, and McInerney DP (2001) Stability of atmospheric CO₂ levels across the Triassic/Jurassic boundary. *Nature* 411: 675–677.

Tanner T, Hernández-Almeida I, Drury AJ, Guitián J, and Stoll H (2020) Decreasing Atmospheric CO₂ During the Late Miocene Cooling. *Paleoceanography and Paleoclimatology* 35. e2020PA003925.

The Cenozoic CO2 Proxy Integration Project (CenCO2PIP) Consortium (2023) Towards a Cenozoic history of atmospheric CO₂. *Science* 382: 6675. https://doi.org/10.1126/science.adi51.

Tierney JE, Poulsen CJ, Montañez IP, Bhattacharya T, and Feng R (2020) The future of past climates. *Science* 370: 6517. https://doi.org/10.1126/science.aay3701.

Tipple BJ, Meyers SR, and Pagani M (2010) Carbon isotope ratio of Cenozoic CO₂: A comparative evaluation of available geochemical proxies. *Paleoceanography* 25: PA3202.

Torres MA, West AJ, and Li G (2014) Sulphide oxidation and carbonate dissolution as a source of CO₂ over geological timescales. *Nature* 507: 346–349.

Tripathy KP, Mukherjee S, Mishra A, Mann ME, and Park Williams A (2023) Climate change will accelerate the high-end risk of compound drought and heatwave events. *Proceedings of the National Academy of Sciences* 120. https://doi.org/10.1073/pnas.2219825120.

Turgeon SC and Creaser RA (2008) Cretaceous Oceanic Anoxic Event 2 triggered by a massive magmatic episode. *Nature* 454: 323–329.

UNFCCC (2015) *UNFCCC Adoption of the Paris Agreement. I: Proposal by the President. Draft Decision CP.21*. United Nations Office, Geneva. https://unfccc.int/resource/docs/2015/cop21/eng/l09r01.pdf.

Urey HC (1952) *The Planets: Their Origin and Development*. New Haven: Yale University Press.

Vajda V and McLoughlin S (2007) Extinction and recovery patterns of the vegetation across the Cretaceous-Paleogene boundary – a tool for unravelling the causes of the end-Permian mass-extinction. *Review of Palaeobotany and Palynology* 144: 99–112. https://doi.org/10.1016/j.revpalbo.2005.09.007.

Vajda V, McLoughlin S, Mays C, Frank TD, Fielding CR, Tevyaw A, Lehsten V, Bocking M, and Nicoll RS (2020) End-Permian (252 Mya) deforestation, wildfires and flooding—An ancient biotic crisis with lessons for the present. *Earth and Planetary Science Letters* 529. 115875.

Valdes PJ, Scotese CR, and Lunt DJ (2021) Deep ocean temperatures through time. *Climate of the Past* 17: 1483–1506. https://doi.org/10.5194/cp-17-1483-2021.

van der Meer D, Zeebe RE, van Hinsbergen D, Sluijs A, Spakman W, and Torsvik TH (2014) Plate tectonic controls on atmospheric CO₂ levels since the Triassic. *Proceedings of the National Academy of Sciences* 111: 4380–4385. https://doi.org/10.1073/pnas.1315657111.

Walker JCG, Hays PB, and Kasting JF (1981) A negative feedback mechanism for the long-term stabilization of Earth's surface temperature. *Journal of Geophysical Research* 86: 9776–9782. https://doi.org/10.1029/JC086iC10p09776.

Wan C, Wang D, Zhu Z, and Quan C (2011) Trend of Santonian (Late Cretaceous) atmospheric CO₂ and global mean land surface temperature: Evidence from plant fossils. *Science China Earth Sciences* 54: 1338–1345. https://doi.org/10.1007/s11430-011-4267-1.

Westerhold T, Marwan N, Drury AJ, Liebrand D, Agnini C, et al. (2020) An astronomically dated record of Earth's climate and its predictability over the last 66 million years. *Science* 369: 1383. https://doi.org/10.1126/science.aba685.

Whiteside JH, Lindstrom S, Irmis RB, Glasspool IJ, Schaller MF, Dunlavey M, Nesbitt SJ, Smith ND, and Turner AH (2015) Extreme ecosystem instability suppressed tropical dinosaur dominance for 30 million years. *Proceedings of the National Academy of Sciences* 112: 7909–7913. https://doi.org/10.1073/pnas.1505252112.

Wilkes EB and Pearson A (2019) A general model for carbon isotopes in red-lineage phytoplankton: Interplay between unidirectional processes and fractionation by RubisCO. *Geochimica et Cosmochimica Acta* 265: 163–181.

Witkowski CR, Weijers JWH, Blais B, Schouten S, and Sinninghe Damsté JS (2018) Molecular fossils from phytoplankton reveal secular pCO₂ trend over the Phanerozoic. *Science Advances* 4: eaat4556. https://doi.org/10.1126/sciadv.aat4556.

Wong TE, Cui Y, Royer DL, and Keller K (2021) A tighter constraint on Earth-system sensitivity from long-term temperature and carbon-cycle observations. *Nature Communications* 12: 3173. https://doi.org/10.1038/s41467-021-23543-9.

Woodward FI (1987) Stomatal numbers are sensitive to increases in CO₂ from pre-industrial levels. *Nature* 327: 617–618. https://doi.org/10.1038/327617a0.

Wu J, Ding S, Li Q, Sun B, and Wang Y (2016) Reconstructing paleoatmospheric CO₂ levels based on fossil Ginkgoites from the Upper Triassic and Middle Jurassic in Northwest China. *PalZ* 90: 377–387.

Wu Y, Chu D, Tong J, Song H, Dal Corso J, Wignall PB, Song H, Du Y, and Cui Y (2021) Six-fold increase of atmospheric pCO₂ during the Permian–Triassic mass extinction. *Nature Communications* 12: 2137. https://doi.org/10.1038/s41467-021-22298-7.

Yan DF, Sun BN, Xie SP, Li XC, and Wen WW (2009) Response to paleo atmospheric CO₂ concentration of *Solenites vimineus* (Phillips) Harris (Ginkgophyta) from the Middle Jurassic of the Yaojie Basin, Gansu Province, China. *Science China Earth Sciences* 2009(52): 2029–2039. https://doi.org/10.1007/s11430-009-0181-1.

Yan Y, Bender ML, Brook EJ, Clifford HM, Kemeny PC, et al. (2019) Two-million-year-old snapshots of atmospheric gases from Antarctic ice. *Nature* 574: 663–666. https://doi.org/10.1038/s41586-019-1692-3.

Yapp CJ (2004) Fe(CO3)OH in goethite from a mid-latitude North American Oxisol: Estimate of atmospheric CO2 concen-tration in the Early Eocene "climatic optimum". *Geochimica et Cosmochimica Acta* 68: 935–947.

Yapp CJ and Poths H (1996) Carbon isotopes in continental weathering environments and variations in ancient atmospheric CO₂ pressure. *Earth and Planetary Science Letters* 137: 71–82.

Yoitis C and McElwain JC (2019) A novel hypothesis for the role of photosynthetic physiology in shaping macroevolutionary patterns. *Plant Physiology* 181: 1148–1162. https://doi.org/10.1104/pp.00749.

Young SA, Saltzman MR, Foland KA, Linder JS, and Kump LR (2009) A major drop in seawater 87Sr/86Sr during the Middle Ordovician (Darriwilian): Links to volcanism and climate? *Geology* 37(10): 951–954.

Zachos J, Pagani M, Sloan L, Thomas E, and Billups K (2001) Trends, rhythms, and aberrations in global climate 65 Ma to present. *Science* 292: 686–693.

Zhang L, Wang C, Wignall PB, Kluge T, Wan X, Wang Q, and Gao Y (2018) Deccan volcanism caused coupled pCO₂ and terrestrial temperature rises, and pre-impact extinctions in northern China. *Geology* 46: 271–274. https://doi.org/10.1130/G39992.1.

Zhang H-Y, Hartmann H, Gleixner G, Thoma M, and Schwab V (2019a) Carbon isotope fractionation including photosynthetic and post-photosynthetic processes in C3 plants: Low [CO_2] matters. *Geochimica et Cosmochimica Acta* 245: 1–15. https://doi.org/10.1016/j.gca.2018.09.035.

Zhang YG, Pearson A, Benthien A, Dong L, Huybers P, Liu X, and Pagani M (2019b) Refining the alkenone-pCO_2 method I: Lessons from the Quaternary glacial cycles. *Geochimica et Cosmochimica Acta* 260: 177–191.

Zhang L, Yang T, Li W-J, Jia J-W, Mou X-S, Chen Y-Q, Xie S-P, Fan J-J, and Yan D-F (2019c) Reading paleoenvironmental information from Middle Jurassic ginkgoalean fossils in the Yaojie and Baojishan basins, Gansu Province, China. *Geobios* 52: 99–106.

Zhang YG, Henderiks J, and Liu X (2020) Refining the alkenone-pCO_2 method II: Towards resolving the physiological parameter 'b'. *Geochimica et Cosmochimica Acta* 281: 118–134.

Zhou WM, Shi GJ, Zhou ZY, and Wang J (2017) Roof shale flora of Coal Seam 6 from the Asselian (lower Permian) Taiyuan Formation of the Wuda Coalfield, Inner Mongolia and its ecostratigraphic significance. *Acta Geological Sinica (English Edition)* 91: 22–38.

Zhou N, Wang Y, Porter AS, Kurschner WM, Li L, Lu N, and McElwain JC (2020) An inter-comparison study of three stomatal-proxy methods for CO_2 reconstruction applied to early Jurassic Ginkgoales plants. *Palaeogeography Palaeoclimatology Palaeoecology* 542: 109547.

Zhu J, Poulsen CJ, and Tierney JE (2019) Simulation of Eocene extreme warmth and high climate sensitivity through cloud feedbacks. *Science Advances* 5: eaax1874. https://doi.org/10.1126/sciadv.aax1874.

Zhu J, Poulsen CJ, and Otto-Bliesner BL (2020) High climate sensitivity in CMIP6 model not supported by paleoclimate. *Nature Climate Change* 10: 378–379. https://doi.org/10.1038/s41558-020-0764-6.